



NTNU – Trondheim
Norwegian University of
Science and Technology

Borehole Stability: Comparing the Deviation Sensibility of Different Failure Criteria

Gustaf Johan Åstrand

Petroleum Engineering

Submission date: June 2015

Supervisor: Rune Martin Holt, IPT

Norwegian University of Science and Technology
Department of Petroleum Engineering and Applied Geophysics

Abstract

During drilling the down-hole pressure has to be sufficient enough to prevent collapse of the wellbore, while at the same time it cannot exceed the fracture limit. Borehole failure can lead to a stuck pipe situation which is time consuming and costly. Ultimately it can evoke serious economic consequences due to the impending need of abandoning the well. Neither drilling with an unnecessary high wellbore pressure, where the margin between collapse and fracturing is sufficient, is economically viable since it will slow down the rate of penetration. Predicting the required mud weight to avoid collapse is a complex process where formation properties and conditions together with the orientation of the wellbore will affect the outcome.

By modeling the stresses around the wellbore and inserting them into a failure criterion a prediction of the required mud weight can be obtained. Several failure criteria is suggested in the literature. The objective of this thesis is to compare their sensibility to deviation as well as gaining a greater understanding of how to perform required mud weight predictions.

Four different failure criteria have been investigated through simulations performed in PSI. Four different cases were assumed and used as input for the simulations. In order to evaluate the Mogi-Coulomb failure criterion and gain knowledge of mud weight prediction calculations a Matlab program was written by the author. Inclination and azimuth sensibility analyzes were run to investigate the different failure criteria's response to deviation.

The Matlab program provides a user friendly output for all possible wellbore orientations and generates results that coincide with the theory and the PSI simulations. Further more the conducted sensibility analyses and failure criteria comparison reveal a wide disagreement between the different failure criteria regarding the minimum mud weight prediction. In case 1 the Mohr-Coulomb and Mogi-Coulomb failure criteria predict the direction of the minimum horizontal in situ stress to be the most beneficial with respect to avoiding collapse, whereas

the Drucker-Prager and Stassi-D'Alia failure criteria prefer the direction of the maximum horizontal stress. This emphasizes how crucial the choice of failure criteria is for predicting the correct minimum mud weight requirement.

Acknowledgments

The author would like to express the deepest appreciation to his supervisor, Professor Rune Martin Holt for providing guidance when all hope of making the deadline of this thesis was lost. The author also wishes to thank his wicked class mates and roommate at NTNU for giving him 2 awesome years in the beautiful city of Trondheim. Finally the author would like to thank his parents Katrin and Gunnar Åstrand for providing moral support throughout these last 5 years. And thank you Nora for putting up with all my wining, you are the best. I love you guys.

Contents

1	Introduction	1
2	Theory	3
2.1	Stress	4
2.1.1	Rotation of the coordinate system	7
2.1.2	Principal stresses	9
2.1.3	Stress invariants	13
2.1.4	Deviatoric stresses	15
2.1.5	Octahedral stresses	15
2.1.6	Effective stress	16
2.2	Strain	17
2.2.1	Principal strains	19
2.3	Elasticity	20
2.4	Anisotropy	22
3	Rock failure and deformation	23
3.1	Mohr-Coulomb	25
3.2	Drucker-Prager	28
3.3	Modified-Lade	29
3.4	Stassi-D'Alia	30
3.5	Mogi-Coulomb	30
3.6	Hoek-Brown	31
3.7	Griffith	31
4	Drilling	33

4.1	Stresses around a borehole	33
4.2	Mohr-Coulomb borehole failure	35
5	Method	37
5.1	PSI simulations	37
5.1.1	Case 1: Weak shale	38
5.1.2	Case 2a: Triassic shale	39
5.1.3	Case 2b and 2c	40
5.2	Matlab calculations	41
6	Results	47
6.1	Comparing failure criteria in PSI case 1	48
6.1.1	Inclination sensibility case 1	52
6.1.2	Azimuth sensibility for case 1	56
6.2	Matlab results case 1	60
6.3	Case 2a	62
6.3.1	Inclination sensibility case 2a	62
6.3.2	Azimuth sensibility case 2a	66
6.4	Matlab results case 2a	70
6.5	Comparing failure criteria case 2b and 2a	72
6.5.1	Inclination sensibility case 2b	76
6.6	Matlab results case 2b	78
6.7	Comparing failure criteria case 2c and 2a	80
6.7.1	Inclination sensibility case 2c	84
6.8	Matlab results case 2c	86

7	Discussion	89
8	Recommendations	91
9	Conclusion	93
	Appendices	97
	Appendix A Failure criteria comparison	97
A.1	Case 1	97
	Appendix B Matlab scripts	101
B.1	Transformation formulas	101
B.1.1	Tensor set up	101
B.1.2	In situ stress tensor to geographical tensor	101
B.1.3	Geographical stress tensor to wellbore tensor	102
B.2	Stresses around the wellbore	103
B.2.1	General elastic solution	103
B.2.2	Principal stresses	104
B.3	Failure criteria functions	105
B.3.1	Mohr-Coulomb Newton’s method	105
B.3.2	Mohr-Coulomb bisection method	106
B.3.3	Mogi-Coulomb bisection method	107
B.3.4	Bisection method	109
B.4	Main script	110
	Appendix C Rock properties	113

List of Figures

1	Stress explanation.	4
2	Force components.	5
3	Stress components.	6
4	Rotation	8
5	Stresses acting on a plane	10
6	Mohr's circle.	11
7	Mohr's circle (3D).	13
8	Strain.	17
9	Shear Strain.	19
10	Stress states.	23
11	Stress vs. Strain	24
12	Mohr-Coulomb.	27
13	Principal stress transformation.	42
14	Geographical stress transformation.	43
15	Output Matlab calculations.	47
16	Mohr-Coulomb case 1.	48
17	Drucker-Prager vs. Mohr-Coulomb case 1.	49
18	Modified Lade vs. Mohr-Coulomb case 1.	50
19	Stassi-D'Alia vs. Mohr-Coulomb case 1.	51
20	Inclination sensibility $Az = 0^\circ$ case 1.	52
21	Inclination sensibility $Az = 90^\circ$ case 1.	54
22	Azimuth sensibility $Inc = 30^\circ$ case 1.	56
23	Azimuth sensibility $Inc = 60^\circ$ case 1.	58

LIST OF FIGURES

24	Mohr-Coulomb Matlab case 1.	60
25	Mogi-Coulomb Matlab case 1.	61
26	Inclination sensibility $Az = 0^\circ$ case 2a.	62
27	Inclination sensibility $Az = 90^\circ$ case 2a.	64
28	Azimuth sensibility $Inc = 30^\circ$ case 2a.	66
29	Azimuth sensibility $Inc = 60^\circ$ case 2a.	68
30	Mohr-Coulomb Matlab case 2a.	70
31	Mogi-Coulomb Matlab case 2a.	71
32	Mohr-Coulomb case 2b vs 2a.	72
33	Drucker Prager case 2b vs 2a.	73
34	Modified Lade case 2b vs 2a.	74
35	Stassi-D'Alia case 2b vs 2a.	75
36	Inclination sensibility case 2b.	76
37	Mohr-Coulomb Matlab case 2b.	78
38	Mogi-Coulomb Matlab case 2b.	79
39	Mohr-Coulomb case 2c vs 2a.	80
40	Drucker-Prager case 2c vs 2a.	81
41	Modified Lade case 2c vs 2a.	82
42	Stassi-D'Alia case 2c vs 2a.	83
43	Inclination sensibility case 2c.	84
44	Mohr-Coulomb Matlab case 2c.	86
45	Mogi-Coulomb Matlab case 2c.	87
A1	Modified Lade vs. Drucker-Prager case 1.	97
A2	Stassi D'alia vs. Drucker-Prager case 1.	98
A3	Stassi D'alia vs. Modified Lade case 1.	99

List of Tables

1	Mohr-Coulomb fracture	36
2	Mohr-Coulomb collapse	36
3	Case 1 inputs	38
4	Case 2a inputs	39
5	Case 2b and 2c inputs	40
C1	Rock properties	113

1 Introduction

When drilling a well there are two main types of wellbore stability issues that can occur, borehole collapse and fracturing. These two issues are generally associated with a well pressure that is too low or a well pressure that is too high respectively. Wellbore stability problems such as these can lead to time, and ultimately, cost consuming operations. Some examples are: back reaming, freeing stuck pipe, loss of circulation, fishing, sidetracking and so on. In order to avoid stability issues the critical mud pressures need to be predicted. This is done through modeling the stresses around a borehole and combining the result with a rock failure criterion. A rock failure criterion is often derived empirically and so the differences between the prediction of failure between the failure criteria can sometimes be significant.

There are several failure criteria in the literature and this text highlights the most common criteria used in the petroleum industry. The motivation and goal for this thesis is to achieve a better understanding of how the different failure criteria behave when altering the factors affecting it and also to gain more knowledge on how to perform mud weight prediction calculations. The author has mainly focused on parameters that could be changed through good planing and predictions such as the azimuth and inclination of the wellbore. Another goal was to find an easy way to present all possible deviation outcomes for a specific case with regards to the minimum mud weight required to avoid collapse.

In order to fully understand failure of rock this text takes the reader through some basic fundamental theory before it deals with the more complex empirical formulas describing failure of rock. A software provided by SINTEF Research Petroleum called PSI has been used to investigate the different failure criteria's sensibility to deviation. A Matlab program has also been written and used in the investigation. Finlay some results and conclusions extracted from the performed simulations and calculations is presented.

2 Theory

The foundation for all aspect of rock mechanics is elasticity which describes a material's ability to resist and recover form deformation caused by external forces. In rock mechanics a better expression would be a material's response in strain caused by external stress. The simplest type of response is called linear elasticity, which means that the external stress and the resulting strain has a linear relationship. For very small changes in applied stresses nearly all materials, including rocks, behave like a linear elastic material. Therefore rock-, and ultimately, failure mechanics have their origin in the theory of linear elasticity. Although larger changes in stresses will reveal that most types of rock are in-elastic.

2.1 Stress

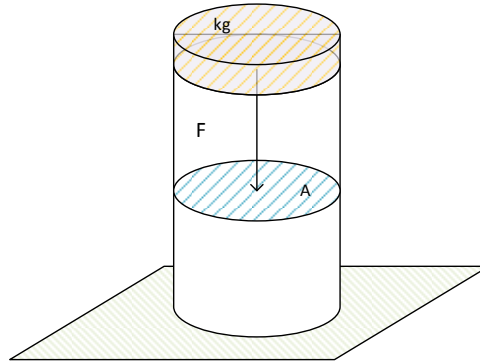


Figure 1: Force and stress relationship.

A common approach to define stress in the literature is to consider a cylinder standing on the ground with a weight placed on top of it (fig. 1). Due to gravity the weight will exert an external force to the cylinder. Since the cylinder is supported by the ground it is still at rest. Following fundamental physics an equal force must also be acting on the cylinder in the reverse direction. Therefore every cross-sections perpendicular to the direction of the force will be exposed to the same force. Hence stress can be defined as:

$$\sigma = \frac{F}{A} \quad (2.1)$$

By writing the equation (2.1) like this might fool the reader to believe that stress is a scalar quantity when in reality it is not. In figure 1 the only force acting on the cross-section area of interest is acting normal towards it, and so for this particular example it is possible to describe the full state of stress with the equation (2.1). By choosing a different area than A , which is carefully chosen to be a perfect cross-section of the cylinder perpendicular to its axis, the state of stress will change. The state of stress is dependent upon the area in which one choose to normalize the force.

Normal stress σ is defined as the force component acting normal to the cross-section area A :

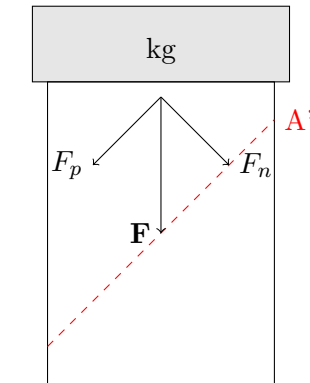


Figure 2: Force components acting on a cross-section.

$$\sigma = \frac{F_n}{A'} \quad (2.2)$$

Shear stress τ is defined as the force component acting parallel to the cross-section area A' :

$$\tau = \frac{F_p}{A'} \quad (2.3)$$

Stress has the unit [Pa]. The general stress convention in mechanics is positive for tensional forces. Since Geo-mechanics often deals with compressional forces the sign convention for stress, σ , is often chosen to be positive when compressive forces are acting on the cylinder and negative when tensile forces are acting on it. The sign convention of the shear stress only effects the direction which often is of lesser concern in rock failure mechanics. Thus τ is often noted $|\tau|$ [Jaeger et al., 2007].

Stress is defined as a point wise quantity. If one were to define a body as a continuum containing an infinite amount of points, then every point would individually have its own value of stress. Thus to describe the complete state of stress at a single point P, one has to imagine three surfaces directed orthogonally to one another.

In figure 3 the stress components related to each surface are described. Phys-

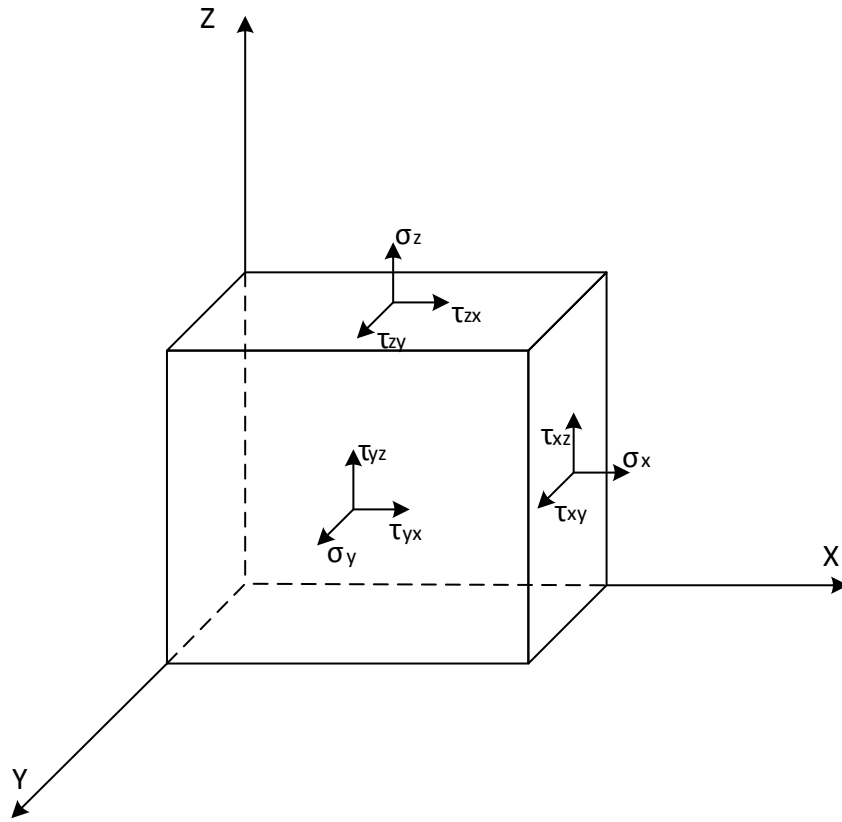


Figure 3: Stress components for a point in space.

ically there will only be one shear stress acting on each surface. By dividing the shear stress into its coordinate components the direction in which the shear stress is acting can be identified. The resulting stress components for point P can then be organized into a matrix:

$$\boldsymbol{\sigma} = \begin{pmatrix} \sigma_x & \tau_{xy} & \tau_{xz} \\ \tau_{yx} & \sigma_y & \tau_{yz} \\ \tau_{zx} & \tau_{zy} & \sigma_z \end{pmatrix} \quad (2.4)$$

When considering a point in an underground formation it is intuitive to conclude that it is at rest, therefore no translational and rotational forces are acting on it. The tensor in equation (2.4) can then be simplified because τ_{ij} will be equal to τ_{ji} . The stress related to a surface normal to the x-axis

is therefore denoted σ_x , τ_{xy} and τ_{xz} . For a surface normal to the y-axis, the related stresses are denoted σ_y , τ_{xy} , τ_{yz} . And similarly, the related stresses to a surface normal to the z-axis are: σ_z , τ_{xz} , τ_{yz} . The simplified tensor, which now has six individual components instead of nine, is shown in equation (2.5).

$$\begin{pmatrix} \sigma_x & \tau_{xy} & \tau_{xz} \\ \tau_{xy} & \sigma_y & \tau_{yz} \\ \tau_{xz} & \tau_{yz} & \sigma_z \end{pmatrix} \quad (2.5)$$

For more complex mathematical derivations the notation in equation (2.5) becomes somewhat impractical. σ_{ij} is then a more practical way to denote both the normal stresses and the shear stresses:

$$\begin{pmatrix} \sigma_{11} & \sigma_{12} & \sigma_{13} \\ \sigma_{12} & \sigma_{22} & \sigma_{23} \\ \sigma_{13} & \sigma_{23} & \sigma_{33} \end{pmatrix} \quad (2.6)$$

2.1.1 Rotation of the coordinate system

The stress tensor is a complete description of the state of stress in a certain coordinate system. If one wants to change the reference frame (rotate the coordinate system) the stress tensor will change according to this new reference frame. For instance it might be convenient to express the state of stress from a deviated wellbores perspective.

In figure 4 the coordinate system is first rotated around the z-axis which points into the paper. That gives that $z=z'$. The value of x' and y' then becomes:

$$x' = \cos(\alpha)x + \sin(\alpha)y \quad (2.7)$$

$$y' = -\sin(\alpha)x + \cos(\alpha)y \quad (2.8)$$

$$z' = z \quad (2.9)$$

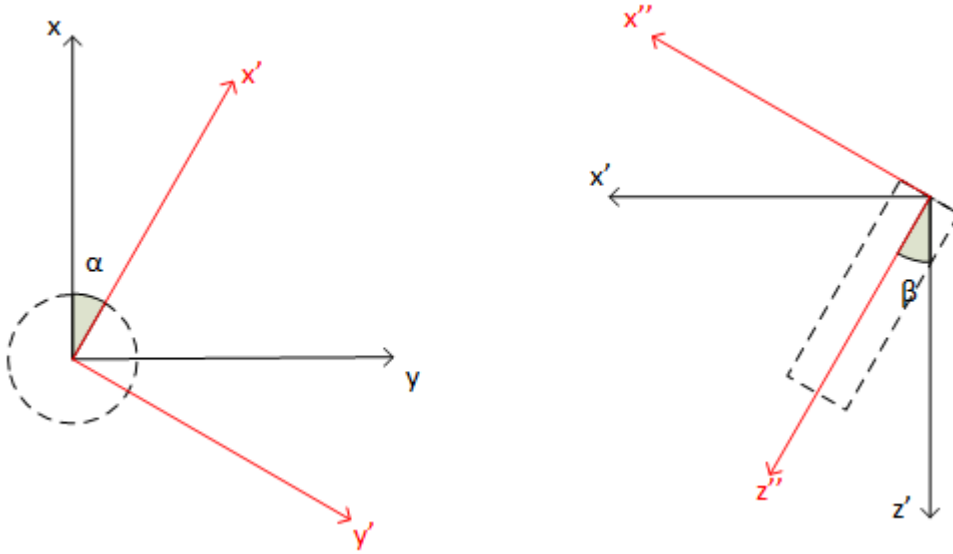


Figure 4: Broken down rotation.

Written in matrix form that yields:

$$\begin{Bmatrix} x' \\ y' \\ z' \end{Bmatrix} = \begin{bmatrix} \cos \alpha & \sin \alpha & 0 \\ -\sin \alpha & \cos \alpha & 0 \\ 0 & 0 & 1 \end{bmatrix} \begin{Bmatrix} x \\ y \\ z \end{Bmatrix} \quad (2.10)$$

Next a new rotation around the y' -axis is performed. Following the same procedure as above y' must equal y'' :

$$x'' = \cos(\beta)x' - \sin(\beta)z' \quad (2.11)$$

$$y'' = y' \quad (2.12)$$

$$z'' = \sin(\beta)x' + \cos(\beta)z' \quad (2.13)$$

$$\begin{Bmatrix} x'' \\ y'' \\ z'' \end{Bmatrix} = \begin{bmatrix} \cos \beta & 0 & -\sin \beta \\ 0 & 1 & 0 \\ \sin \beta & 0 & \cos \beta \end{bmatrix} \begin{Bmatrix} x' \\ y' \\ z' \end{Bmatrix} \quad (2.14)$$

When inserting equation (2.10) into equation (2.14) the following equation is obtained:

$$\begin{Bmatrix} x'' \\ y'' \\ z'' \end{Bmatrix} = \begin{bmatrix} \cos \beta & 0 & -\sin \beta \\ 0 & 1 & 0 \\ \sin \beta & 0 & \cos \beta \end{bmatrix} \begin{bmatrix} \cos \alpha & \sin \alpha & 0 \\ -\sin \alpha & \cos \alpha & 0 \\ 0 & 0 & 1 \end{bmatrix} \begin{Bmatrix} x \\ y \\ z \end{Bmatrix} \quad (2.15)$$

Which can be written:

$$\begin{Bmatrix} x'' \\ y'' \\ z'' \end{Bmatrix} = \begin{bmatrix} \cos(\alpha) \cos(\beta) & \sin(\alpha) \cos(\beta) & -\sin \beta \\ -\sin(\alpha) & \cos(\alpha) & 0 \\ \cos(\alpha) \sin(\beta) & \sin(\alpha) \sin(\beta) & \cos \beta \end{bmatrix} \begin{Bmatrix} x \\ y \\ z \end{Bmatrix} \quad (2.16)$$

The 3×3 matrix in equation (2.16) is called a rotation matrix. If one were to rotate the coordinate system around the third and final axis the rotation matrix will contain a third variable. This rotation matrix is given in equation (5.1) in chapter 5.2. How to transform a stress tensor is also explained in this chapter.

2.1.2 Principal stresses

Failure of rock often occur along a plane. Finding the corresponding normal and shear stress of any plane thus become essential. In figure 5 several forces are acting on a triangle in the xy -plane. Since the triangle is at rest all the forces are at equilibrium. Solving for the normal and shear stress on the 'hypotenuse' surface we get the two equations:

$$\sigma = \frac{1}{2}(\sigma_x + \sigma_y) + \frac{1}{2}(\sigma_x - \sigma_y)\cos 2\theta + \tau_{xy}\sin 2\theta \quad (2.17)$$

$$\tau = \frac{1}{2}(\sigma_y - \sigma_x)\sin 2\theta + \tau_{xy}\cos 2\theta \quad (2.18)$$

From equation (2.18) we can find the angles θ where the shear stress disappears ($\tau = 0$):

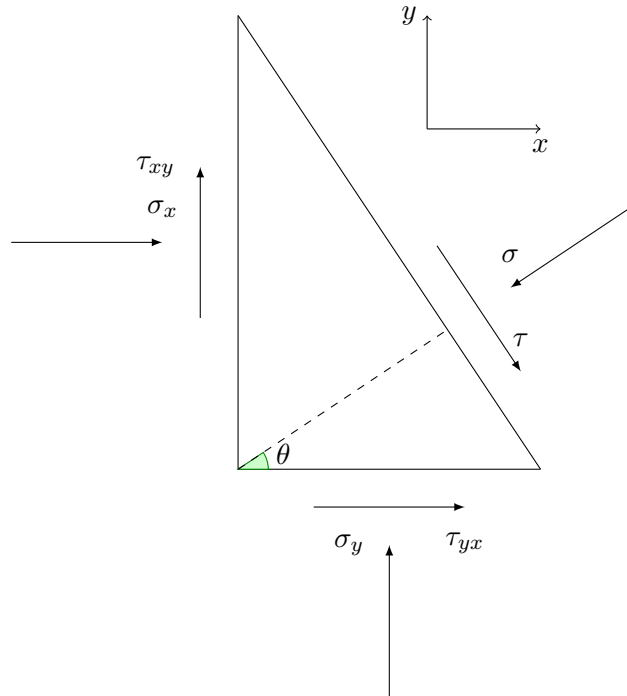


Figure 5: Normal stress and shear stress acting on a plane.

$$\tan 2\theta = \frac{2\tau_{xy}}{\sigma_x - \sigma_y} \quad (2.19)$$

Equation (2.19) has two solutions, $\theta_{1,2}$, which are two different directions. “These two directions are called the *principal axes of stress*” [Fjær et al., 2008, p. 8] which are perpendicular to each other, and the normal stresses corresponding to these directions are found by combining the equations (2.19) and (2.17):

$$\sigma_{1,2} = \frac{\sigma_x + \sigma_y}{2} \pm \frac{\sqrt{(\sigma_x - \sigma_y)^2 + \tau_{xy}^2}}{2} \quad (2.20)$$

Where the notation $\sigma_1 \geq \sigma_2$ is chosen for convenience.

Now imagine that the coordinate system in figure 5 is rotated counterclockwise from the x-direction with the angle θ so that the normal σ and shear

stress τ become parallel with one coordinate axis each. From the equations (2.17) and (2.18) one can see that the normal and shear stresses in the $\sigma\tau$ -plane can be represented as:

$$\sigma = \frac{1}{2}(\sigma_1 + \sigma_2) + \frac{1}{2}(\sigma_1 - \sigma_2)\cos 2\theta \quad (2.21)$$

$$\tau = -\frac{1}{2}(\sigma_1 - \sigma_2)\sin 2\theta \quad (2.22)$$

By representing the stresses in the $\sigma\tau$ -plane, the so called *Mohr's circle* is obtained (figure 6). From equation (2.21) the center of the circle is found at $(\sigma_1 + \sigma_2)/2$. The circle has a radius of $(\sigma_1 - \sigma_2)/2$ as seen from equation (2.21) and (2.22).

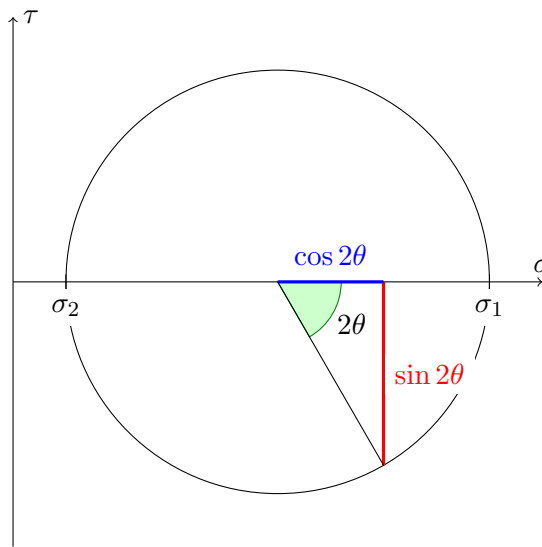


Figure 6: Mohr's circle representing the normal and shear stress for any angle θ of cross section plane.

The method of finding the principal stresses in three-dimensions follows the same steps as in two dimensions. The stresses in a three-dimensional space, defined in equation (2.5), are combined with a way to determine how to identify a direction in space. "This can be done by the direction cosines" [Fjær et al., 2008, p. 8]:

$$l_x = \cos \alpha_x \quad (2.23)$$

$$l_y = \cos \alpha_y \quad (2.24)$$

$$l_z = \cos \alpha_z \quad (2.25)$$

$$(2.26)$$

Then solving for σ in the determinant equation:

$$\begin{vmatrix} \sigma_x - \sigma & \tau_{xy} & \tau_{xz} \\ \tau_{xy} & \sigma_y - \sigma & \tau_{yz} \\ \tau_{xz} & \tau_{yz} & \sigma_z - \sigma \end{vmatrix} = 0 \quad (2.27)$$

This yields three solutions, namely: σ_1 , σ_2 and σ_3 . Following the same principal as in equation (2.20), the notation of the solutions are organized in such way that $\sigma_1 \geq \sigma_2 \geq \sigma_3$. To be able to find the direction of the principal axis corresponding to the principal stress σ_i the directional cosines l_{ix} , l_{iy} and l_{iz} are found by solving the equations:

$$l_{ix}(\sigma_x - \sigma_i) + l_{iy}\tau_{xy} + l_{iz}\tau_{xz} = 0 \quad (2.28)$$

$$l_{ix}\tau_{xy} + l_{iy}(\sigma_y - \sigma_i) + l_{iz}\tau_{yz} = 0 \quad (2.29)$$

$$l_{ix}\tau_{xz} + l_{iy}\tau_{yz} + l_{iz}(\sigma_z - \sigma_i) = 0 \quad (2.30)$$

From the equations (2.28) - (2.30) one can then conclude that principal stresses are orthogonal. It is interesting to note that when the coordinate system is orientated so that the x-axis is parallel to the minimum principals axis, the y-axis is parallel to the intermediate principal axis and the z-axis parallel to the maximum principal axis, the stress tensor has the simple form:

$$\begin{pmatrix} \sigma_3 & 0 & 0 \\ 0 & \sigma_2 & 0 \\ 0 & 0 & \sigma_1 \end{pmatrix} \quad (2.31)$$

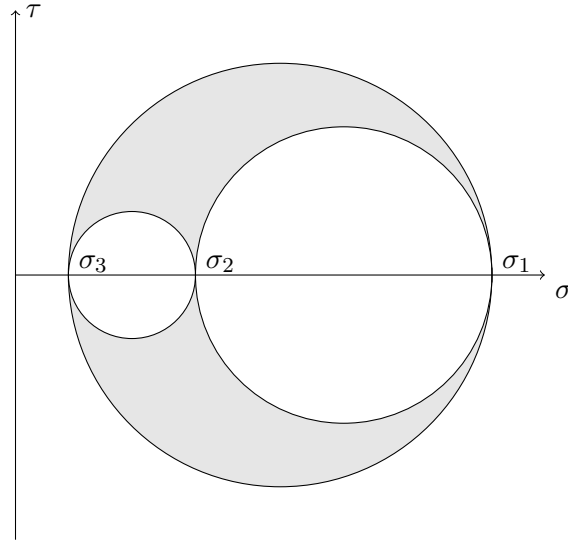


Figure 7: Mohr's circle in three dimensions.

Mohr's circle representing three-dimensional stress states ($\sigma_1 > \sigma_2 > \sigma_3$) are more complicated to derive. [Jaeger et al., 2007, p. 35] is a good source for the curious reader. Figure 7 shows a basic representation where the normal and shear stress for all directions can be found on the edge of every circle or the gray area.

2.1.3 Stress invariants

In wellbore stability analysis it is common to re-orientate the coordinate system in such way that the z-axis is parallel to the axial direction of the wellbore. Doing this means that the components of the stress tensor will change (see chapter 2.1.1). Some properties of the tensor will however remain unchanged, these are called invariants of stress. When expanding the determinant equation (2.27) it takes the form:

$$\sigma^3 - I_1\sigma^2 - I_2\sigma - I_3 = 0 \quad (2.32)$$

where

$$I_1 = \sigma_x + \sigma_y + \sigma_z \quad (2.33)$$

$$I_2 = \tau_{xy}^2 + \tau_{yz}^2 + \tau_{xz}^2 - \sigma_x\sigma_y - \sigma_y\sigma_z - \sigma_x\sigma_z \quad (2.34)$$

$$I_3 = \sigma_x\sigma_y\sigma_z + 2\tau_{xz}\tau_{yz}\tau_{xz} - \sigma_x\tau_{yz}^2 - \sigma_y\tau_{xz}^2 - \sigma_z\tau_{xy}^2 \quad (2.35)$$

These coefficients are an example of stress invariants. They have the same value in all coordinate systems. There are many stress combinations that form invariants of the stress tensor, but only I_1 , I_2 and I_3 are truly independent. This means that any other invariant of the stress tensor depends upon the set I_1 , I_2 and I_3 . When expressed in a orthogonal principal stress coordinate system the invariants take on a simpler form:

$$I_1 = \sigma_1 + \sigma_2 + \sigma_3 \quad (2.36)$$

$$I_2 = -(\sigma_1\sigma_2 + \sigma_2\sigma_3 + \sigma_1\sigma_3) \quad (2.37)$$

$$I_3 = \sigma_1\sigma_2\sigma_3 \quad (2.38)$$

Note that the mean normal stress can be expressed as:

$$\bar{\sigma} = \frac{1}{3}(\sigma_x + \sigma_y + \sigma_z) = \frac{1}{3}I_1 \quad (2.39)$$

hence, the mean normal stress is an invariant and ultimately its value will not change when changing a coordinate system into a rotated set of coordinate axes. [Jaeger et al., 2007].

2.1.4 Deviatoric stresses

The stress tensor in equation (2.5) can be broken down into two components:

$$\boldsymbol{\sigma} = \begin{pmatrix} \bar{\sigma} & 0 & 0 \\ 0 & \bar{\sigma} & 0 \\ 0 & 0 & \bar{\sigma} \end{pmatrix} + \begin{pmatrix} \sigma_x - \bar{\sigma} & \tau_{xy} & \tau_{xz} \\ \tau_{xy} & \sigma_y - \bar{\sigma} & \tau_{yz} \\ \tau_{xz} & \tau_{yz} & \sigma_z - \bar{\sigma} \end{pmatrix} \quad (2.40)$$

The first component containing the mean normal stress is the isotropic part of the stress tensor. This component essentially causes uniform compression or extension. The second component is the deviatoric part which causes distortion. Deviatoric stress is often noted as:

$$\mathbf{S} = \begin{pmatrix} \sigma_x - \bar{\sigma} & \tau_{xy} & \tau_{xz} \\ \tau_{xy} & \sigma_y - \bar{\sigma} & \tau_{yz} \\ \tau_{xz} & \tau_{yz} & \sigma_z - \bar{\sigma} \end{pmatrix} = \begin{pmatrix} S_x & S_{xy} & S_{xz} \\ S_{xy} & S_y & S_{yz} \\ S_{xz} & S_{yz} & S_z \end{pmatrix} \quad (2.41)$$

Many failure criteria are concerned primarily with distortion. Therefore it is useful to express the deviatoric stress in terms of its invariants:

$$J_1 = S_x + S_y + S_z = 0 \quad (2.42)$$

$$J_2 = S_{xy}^2 + S_{xz}^2 + S_{yz}^2 - S_x S_y - S_x S_z - S_y S_z \quad (2.43)$$

$$J_3 = S_x S_y S_z + 2S_{xz} S_{yz} S_{xz} - S_x S_{yz}^2 - S_y S_{xz}^2 - S_z S_{xy}^2 \quad (2.44)$$

2.1.5 Octahedral stresses

The normal and shear stresses acting on planes normal to the $(\pm 1, \pm 1, \pm 1)$ directions in the principal stress space are called octahedral stresses since there are eight such planes (in rock mechanics the direction of most interest is often $(1, 1, 1)$). This plane is referred to as the octahedral-, π - or deviatoric plane [Fjær et al., 2008]. The octahedral stresses are given by:

$$\tau_{oct} = \frac{1}{3} \sqrt{(\sigma_2 - \sigma_3)^2 + (\sigma_3 - \sigma_1)^2 + (\sigma_1 - \sigma_2)^2} = \sqrt{\frac{2}{3}} J_2 \quad (2.45)$$

$$\sigma_{oct} = \frac{1}{3}(\sigma_1 + \sigma_2 + \sigma_3) = \bar{\sigma} = \frac{1}{3} I_1 \quad (2.46)$$

2.1.6 Effective stress

Rocks are a in general porous material to some extent. In underground formations these pores are filled with fluids (gas, oil, water or a mixture of these) under pressure. The pore fluid may affect the rock strength mechanically or chemically. The mechanical effect of the pore pressure is generally of more concern within failure mechanics. Pore pressure acts outward from the pore space in all directions, hence pore pressure can be thought of as a tensile strength weakening the rock:

$$\sigma'_i = \sigma_i - p_p \quad (2.47)$$

p_p is the pore fluid pressure. In the literature the pore pressure is often multiplied by a coefficient α called the *effective stress coefficient* or the Biot coefficient. The effective stress coefficient in unconsolidated or weak rocks are ≈ 1 . In failure mechanics the Biot coefficient should be assumed to be equal to one [Gueguen and Bouteica, 1999], therefore it won't be discussed further in this thesis. Equation (2.47) physically means that the solid frame work of the rock supports the σ'_i part of the total external stress σ_i , whereas the pore fluid pressure p_p supports the rest of σ_i . The pore pressure only affect the normal stresses which means that the “effective” shear stresses are identical to the actual shear stress. [Jaeger et al., 2007]. Thus the effective stress tensor can be written:

$$\boldsymbol{\sigma}' = \begin{pmatrix} \sigma'_x & \tau_{xy} & \tau_{xz} \\ \tau_{xy} & \sigma'_y & \tau_{yz} \\ \tau_{xz} & \tau_{yz} & \sigma'_z \end{pmatrix} \quad (2.48)$$

2.2 Strain

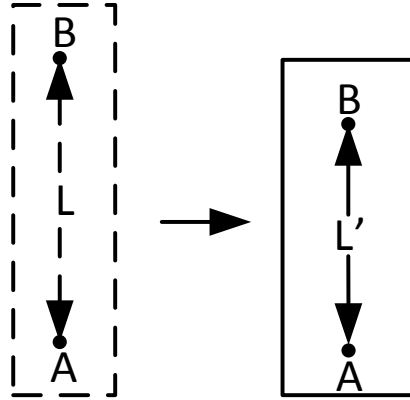


Figure 8: Deformation of a body.

Theory of solid mechanics generally deals with stresses and *strain*, ε , rather than forces and displacement. Strain is a measure of relative change of displacement of nearby particles. If a one-dimensional rod with the length L is deformed to the new length L' , then the mean strain undergone by the rod is defined as the fractional decrease in the length of the rod [Jaeger et al., 2007].

$$\varepsilon = \frac{L - L'}{L} \quad (2.49)$$

In figure 8 the body's initial (dashed) state is strained. The displacement between point A and B in the direction of AB is elongated. It is this particular type of elongation displacement that correctly is defined as strain. Since compressional stress is positive in Geo-mechanics then, to be consistent, the sign convention of strain will be positive if the length of the rod decreases.

In figure 9 the direction of AC is changed from the body's initial state. This type of strain is defined as shear strain:

$$\Gamma = \frac{1}{2} \tan \Psi \quad (2.50)$$

Strain and shear strain can be generalized in more complex problems con-

cerning more than one dimension. Elementary mathematics describe normal and shear strain in the same manor as stresses can be represented. [Jaeger et al., 2007, p. 48] [Fjær et al., 2008, p. 17]:

$$\boldsymbol{\varepsilon} = \begin{pmatrix} \varepsilon_x & \Gamma_{xy} & \Gamma_{xz} \\ \Gamma_{xy} & \varepsilon_y & \Gamma_{yz} \\ \Gamma_{xz} & \Gamma_{yz} & \varepsilon_z \end{pmatrix} \quad (2.51)$$

In equation (2.51) the strains are organised in a tensor. Again, for more complex mathematical derivations ε_{ij} is a more useful notation to denote both the normal and shear strains:

$$\begin{pmatrix} \varepsilon_{11} & \varepsilon_{12} & \varepsilon_{13} \\ \varepsilon_{12} & \varepsilon_{22} & \varepsilon_{23} \\ \varepsilon_{13} & \varepsilon_{23} & \varepsilon_{33} \end{pmatrix} \quad (2.52)$$

In chapter 2.1.3 it is shown that the trace of a matrix does not change in magnitude for any rotation. Thus the the trace is in fact an invariant. The trace of the matrix in equation (2.51) equals the relative decrease in volume, also called the volumetric strain:

$$\varepsilon_{vol} = \varepsilon_x + \varepsilon_y + \varepsilon_z \quad (2.53)$$

The volumetric strain can also be expressed more implicitly [Jaeger et al., 2007]:

$$\varepsilon_{vol} = -\frac{dV}{V} \quad (2.54)$$

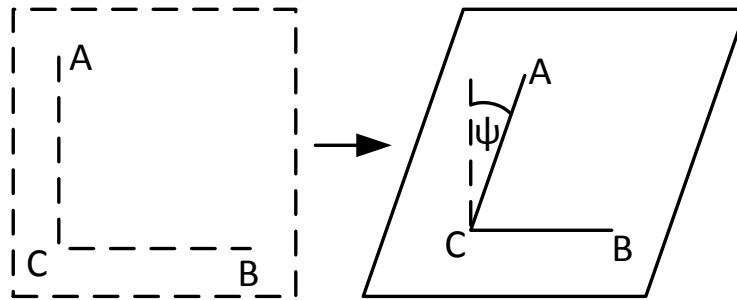


Figure 9: Shear deformation of a body.

2.2.1 Principal strains

Following the method of finding the principal stresses in chapter 2.1.2 one can find the principal strains. In three dimensions there are three orthogonal directions in which the shear stresses will equal zero. The resulting elongation along these principal axes of strain are called the principal strains [Fjær et al., 2008]. Exchanging the stresses and shear stresses in the determinant equation (2.27) with the corresponding strains and shear strains yields the principal strains ε_1 , ε_2 and ε_3 . The principal axes of strain are then found by following the same procedure as in the equations (2.28) - (2.30).

2.3 Elasticity

Elasticity is defined as a material's ability to withstand and recover from deformation caused by forces. In rock mechanics this ultimately comes down to the relationship between stress and strain. When the strain increases linearly with stress the material is said to show linearly elastic behavior. When the change in force is small, almost all rock types show a linear response. Thus linear elasticity is fundamental for further discussion regarding elasticity [Fjær et al., 2008].

$$\sigma_i = \frac{1}{E} \varepsilon_i \quad (2.55)$$

Equation (2.55) is called Hooke's law. E is the *Young's modulus* and it is a so called *elastic moduli* coefficient which is a group of coefficients that measures the stiffness of materials. E has the units of [Pa].

When a specimen is under uniaxial compression not only will strain act on it vertically, but also horizontally. When pressing a tennis ball to the ground the height of it decreases, but the width increases. Rocks behave in a similar way, although due to sedimentary rocks' porous nature the rate of height decrease vs. width increase will not be the same as for the tennis ball's. This type of ratio can be expressed as:

$$v = -\frac{\varepsilon_j}{\varepsilon_i} \quad (2.56)$$

v is called the Poisson's ratio. The two equations above describe two linear elastic constants (or elastic moduli) for a situation where σ_i is the only component causing the strain. In other words, σ_j and σ_k equals zero. Several other elastic moduli that measure the materials stiffness exists and for a linear elastic material they can all be related to one another. [Jaeger et al., 2007, p. 108] is a good source for the curious reader. The simplified method of describing the elastic response of a material in the equations (2.55) and (2.56) coincide with the generalized and simplified way to describe stress in

equation (2.1) and strain in equation (2.49).

To fully describe an isotropic linear elastic material's stress strain relationship, making use of the stress tensors explained in equation (2.6) and (2.52), the following notation can be used:

$$\sigma_{ij} = \lambda \varepsilon_{vol} \delta_{ij} + 2G \varepsilon_{ij} \quad \delta_{ij} \equiv \begin{cases} 1 & \text{if } i = j \\ 0 & \text{if } i \neq j \end{cases} \quad (2.57)$$

where λ and G are elastic moduli known as Lamé's parameters. δ is the Kronecker symbol [Fjær et al., 2008]. Writing the full stress tensor for an isotropic linear elastic material thus reveal:

$$\boldsymbol{\sigma} = \begin{pmatrix} \lambda \varepsilon_{vol} + 2G \varepsilon_{11} & 2G \varepsilon_{12} & 2G \varepsilon_{13} \\ 2G \varepsilon_{12} & \lambda \varepsilon_{vol} + 2G \varepsilon_{22} & 2G \varepsilon_{23} \\ 2G \varepsilon_{13} & 2G \varepsilon_{23} & \lambda \varepsilon_{vol} + 2G \varepsilon_{33} \end{pmatrix} \quad (2.58)$$

2.4 Anisotropy

Elasticity calculations of rocks often assumes that rocks are an isotropic material, meaning that within the rock there is an infinite number of symmetric planes. This, however, is not true for most rocks which often are anisotropic to some extent. The elastic moduli of the rock will then depend on the orientation of the rock. Sedimentary rocks are created through a dispositional system of some kind and due to the non-random nature of sediment deposition the final structures of sedimentary rocks are not homogeneous. Shale formations, for instance, tend to have a layered structure which intensifies the anisotropic response in stress tests. This type of anisotropy is called *intrinsic* or lithological. Another type of anisotropy in rock mechanics is due to the external stresses. A rock that previously may have been isotropic has, due to anisotropic external stresses, now developed micro cracks within its structure. This type of anisotropy is called *induced* anisotropy. [Jaeger et al., 2007].

Historically rocks have mainly been treated as an isotropic material when performing rock elasticity calculations. This is not completely due to the complexity that anisotropy brings, but also that many properties required for performing anisotropy calculations are not always possible to obtain. Keeping in mind that most sedimentary rocks are anisotropic will then give an explanation to some large errors that can be obtained in elasticity calculations when assuming the rock to behave as a linear elastic material.

3 Rock failure and deformation

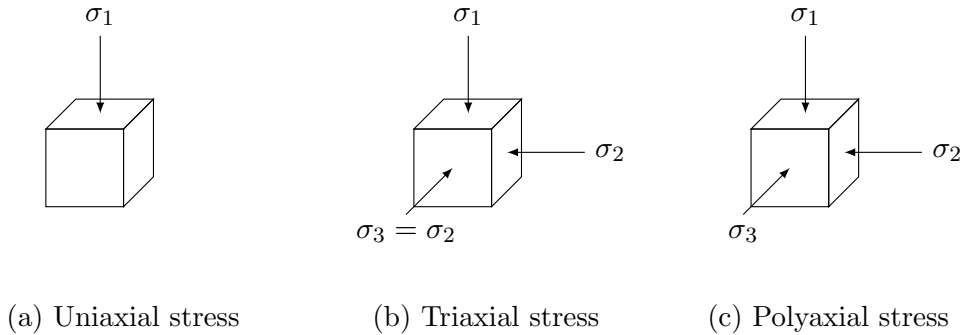


Figure 10: Cubic specimen under different states of stress.

Mechanical properties of rocks have mainly been derived from empirical observations of axial compression tests. In figure 10a the confining pressure equals zero. The cubic specimen is therefore said to be under uniaxial compression. Figure 10b shows a cubic specimen under the stress state where $\sigma_1 > \sigma_2 = \sigma_3$, which is referred to triaxial compression. In general these two tests are conducted on a cylindrical rock sample where the height vs. diameter ratio is 2:1. A pair of pistons apply the axial stress, whereas the confining stresses are applied by some fluid (usually oil) under pressure. Historically these are the most common compression test in rock mechanics due to the fact that most available rock samples are obtained from drillout core samples. Polyaxial (or true triaxial) compression tests (fig. 10c), where $\sigma_1 > \sigma_2 > \sigma_3$, are performed on cubic specimen.

Figure 11 shows a typical result from a uniaxial compression test plotted in a stress vs. strain graph. Several important rock properties can be obtained from such a test. Uniaxial compressive strength (peak stress) C_0 , is one of them. Furthermore the plot can be divided into different regions. In the elastic region the rock deforms elastically, which means that when it is released from stress the specimen will return to its original state. When the stress strain relationship starts to show a downward concave curve the rock is said to be past its yield point. The rock is now in the ductile region which means that when stress is released the rock will have obtained perma-

ment deformation, but is still able to support a load. In the brittle region the specimen undergoes serious deformation and rapidly loses its ability to withstand stress. [Jaeger et al., 2007] [Fjær et al., 2008].

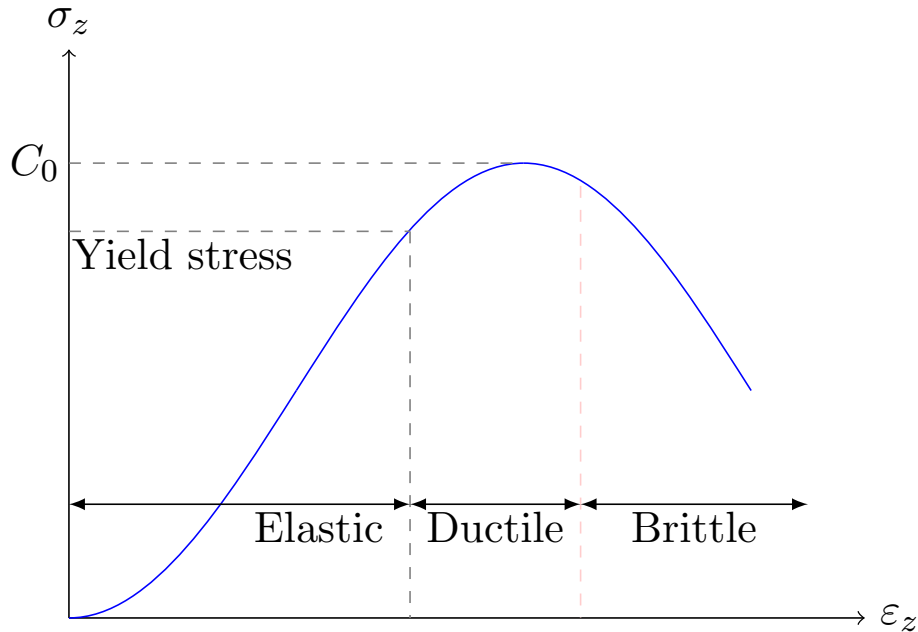


Figure 11: Stress vs. strain in a uniaxial compression test.

The two major wellbore stability issues, collapse and fracturing, occur due to shear failure and tensile failure respectively. Tensile failure for isotropic rocks will occur when the minimum principal stress is overcome. For isotropic rocks the tensile failure criterion becomes:

$$\sigma'_3 = -T_0 \quad (3.1)$$

where T_0 is the tensile strength. For most sedimentary rocks the tensile strength is typically only a few MPa [Fjær et al., 2008]. Different shear failure criteria are discussed in the following sub-chapters.

3.1 Mohr-Coulomb

When the shear stress along some plane in a rock becomes high enough shear failure will occur. Mohr's hypothesis assumes that the critical shear stress τ_{max} depends on the normal stress σ' acting over that failure plane:

$$|\tau_{max}| = f(\sigma') \quad (3.2)$$

In 1776 Coulomb suggested that a compressed rock will fail when the shear stress on a specific plane overcomes the natural cohesion S_0 and the internal friction that opposes motion along that plane. This is the simplest and, still today, most important failure criterion [Al-Ajmi and Zimmerman, 2005]. The criterion simply assumes that $f(\sigma')$ is a linear function of σ' which is a special case of Mohr's hypothesis, hence the criterion is called the Mohr-Coulomb failure criterion:

$$|\tau| = S_0 + \mu\sigma' \quad (3.3)$$

μ is called the *coefficient of internal friction*. Equation (3.3) draws a straight line on the $(\sigma', |\tau|)$ plane and the angle φ that it makes with the σ' axis is called the *angle of internal friction*. φ and μ is related by:

$$\mu = \tan \varphi \quad (3.4)$$

The Mohr-Coulomb criterion can be drawn in the $(\sigma', |\tau|)$ plane by combining the equation (3.3) and the Mohr's circle for the effective principal stresses. According to the Mohr-Coulomb criterion no failure will occur if the Mohr's circle is completely below the failure line. Whereas when the failure line touches the Mohr's circle failure will occur. From figure 12 trigonometry shows that:

$$2\beta = 90^\circ + \varphi \quad \text{or} \quad \beta = 45^\circ + \frac{1}{2}\varphi \quad (3.5)$$

$|\tau|$ implies that there are two possible planes of failure each orientated on either side to the maximum effective principal stress σ'_1 at the acute angle of β . These are the the *conjugate directions* of shear failure [Jaeger et al., 2007, p. 91]. From figure 12 it is possible to derive an equation that represent the Mohr-Coulomb criterion in terms of the effective principal stresses by first replacing the principal stresses σ_i , with the correlating effective principal stresses σ'_i , in the equations (2.21) and (2.22). Second step is to introduce these two equations into equation (3.7), then replace β and μ with φ and derive:

$$\sigma'_1 = 2S_0 \frac{\cos \varphi}{1 - \sin \varphi} + \sigma'_3 \frac{1 + \sin \varphi}{1 - \sin \varphi} \quad (3.6)$$

Inserting $\sigma'_3 = 0$ into equation (3.6) finds the uniaxial compressive strength $C_0 = 2S_0 \tan \beta$ and the Mohr-Coulomb criterion represented in effective principal stress plane becomes:

$$\sigma'_1 = C_0 + \sigma'_3 \tan^2 \beta = C_0 + q\sigma'_3 \quad (3.7)$$

It can sometimes be convenient to re-arrange equation (3.7) in such way that the pore pressure effect is included in a constant. In the following equation it is assumed that the effective stress is represented as in equation (2.47), meaning that the Biot coefficient equals 1:

$$\sigma_1 = C + q\sigma_3 \quad (3.8)$$

$$C = C_0 - p_f(q - 1) \quad (3.9)$$

One convenient way to also express the Mohr-Coulomb criterion is in terms of the maximum shear stress τ_{max} and the effective mean stress $\sigma_{m,2}$ [Jaeger et al., 2007, p. 91]:

$$\tau_{max} = S_0 \cos \varphi + \sigma_{m,2} \sin \varphi \quad (3.10)$$

Where τ_{max} and $\sigma_{m,2}$ can again be seen in the Mohr's circel as:

$$\tau_{max} = \frac{1}{2}(\sigma'_1 - \sigma'_3) \quad (3.11)$$

$$\sigma'_{m,2} = \frac{1}{2}(\sigma'_1 + \sigma'_3) \quad (3.12)$$

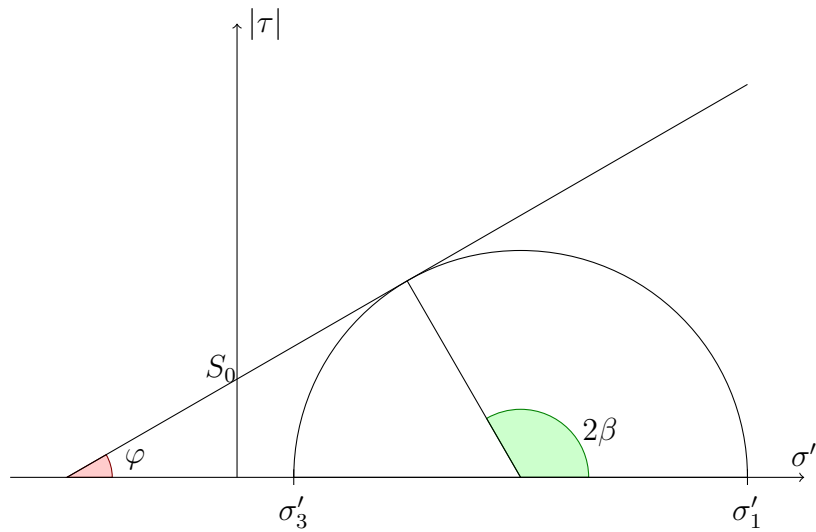


Figure 12: Mohr's Coulomb criterion in the $(\sigma', |\tau|)$ plane.

Even though one can represent the Mohr's circle for three dimension it is clear from figure 7 and equation (3.3) that the Mohr-Coulomb failure criterion neglects the effect of the intermediate principal stress σ'_2 . Mohr-Coulomb can therefore be seen as a two dimensional failure criterion. In three dimensions it is therefore only valid for most rocks when $\sigma_2 = \sigma_3$. In the cross-sectional pi -plane the Mohr-Coulomb failure criteria shows an irregular hexagonal shape with sharp corners and threefold symmetry. The Mohr-Coulomb criterion conservatively overestimates the critical mud pressure for collapse. [Al-Ajmi and Zimmerman, 2006].

3.2 Drucker-Prager

In reality underground formations are often under the stress condition where $\sigma'_1 > \sigma'_2 > \sigma'_3 > 0$. Hence several true-triaxial failure criteria have been proposed for rocks. In 1952, almost 20 years before the first polyaxial compression test apparatus was constructed, Drucker and Prager presented a failure criterion based on the relationship between the second invariant of the deviatoric stress J_2 and the first invariant of stress I_1 [Zhang et al., 2010]:

$$\sqrt{J_2} = k + \alpha I_1 \quad (3.13)$$

where α and k are material constants which can be determined by matching the Drucker-Prager and the Mohr-Coulomb failure criterion for two points in the π -plane. The matching points can be chosen so that the Drucker-Prager failure surface inscribes the hexagonal pyramid of the Mohr-Coulomb failure surface. In that case α and k are related to C_0 and φ in such way that:

$$\alpha = \frac{3 \sin \varphi}{\sqrt{9 + 3 \sin^2 \varphi}} \quad (3.14)$$

$$k = \frac{3C_0 \cos \varphi}{2\sqrt{q}\sqrt{9 + 3 \sin^2 \varphi}} \quad (3.15)$$

where $q = \tan^2 \beta = \tan^2(45^\circ + \frac{1}{2}\varphi)$ from equation (3.7) and (3.5). The circumscribed Drucker-Prager correlates to Mohr-Coulomb in such way that:

$$\alpha = \frac{\sqrt{3}(q - 1)}{q + 2} \quad (3.16)$$

$$k = \frac{\sqrt{3}C_0}{q + 2} \quad (3.17)$$

The Drucker-Prager failure criterion overestimates the strengthening effect of

the intermediate principal strength according to [Al-Ajmi and Zimmerman, 2006] and [Zhang et al., 2010]. Therefore it is not sustainable to estimate the critical mud pressure for collapse from this failure criterion.

3.3 Modified-Lade

The Modified-Lade failure criterion is a three-dimensional modified version of an empirical failure criterion originally formulated by Lade in 1977 [Ewy et al., 1999]:

$$\frac{I_1'^3}{I_3'} - 27 = \eta \quad (3.18)$$

I_1' and I_3' are modified representations of the first and third effective principal stress invariant respectively:

$$I_1' = (\sigma_1' + S_1) + (\sigma_2' + S_1) + (\sigma_3' + S_1) \quad (3.19)$$

$$I_3' = (\sigma_1' + S_1)(\sigma_2' + S_1)(\sigma_3' + S_1) \quad (3.20)$$

S_1 and η are material constants related to the cohesion and internal friction of the rock respectively:

$$S_1 = \frac{S_0}{\tan \varphi} \quad (3.21)$$

$$\eta = 4 \tan^2 \varphi \frac{9 - 7 \sin \varphi}{1 - \sin \varphi} \quad (3.22)$$

S_0 and φ are determined from triaxial compressions tests.

3.4 Stassi-D'Alia

The Stassi-D'Alia failure failure criteria, developed by Fernando Stassi-D'Alia [Stassi-D'Alia, 1967], is used within Statoil “as it has been found to produce results comparable with operational experience” [Kvevik et al., 2013, p. 4]:

$$(\sigma_1 - \sigma_2)^2 + (\sigma_2 - \sigma_3)^2 + (\sigma_3 - \sigma_1)^2 = 2(C_0 - T_0)(\sigma_1 + \sigma_2 + \sigma_3) + 2C_0T_0 \quad (3.23)$$

3.5 Mogi-Coulomb

Comparing triaxial tests with true triaxial test shows that for many rock types σ'_2 has an effect on rock strength. Mogi found that the intermediate principal stress does indeed have an impact on rock strength [Mogi, 1971]. He conducted extensive polyaxial tests and observed that brittle failure occurs along a plane striking in the intermediate principal stress direction. From this he concluded that the mean normal stress (3.12) opposes the creation of a fracture. Hence he assumed that the critical stress τ_{oct} for which failure occurs depend on the mean normal stress $\sigma_{m,2}$:

$$\tau_{oct} = f(\sigma_{m,2}) \quad (3.24)$$

where f is some function. In 2004, based on Mogi's assumption, Al-Ajmi and Zimmerman developed a failure criterion that could predict polyaxial behavior from triaxial tests [Al-Ajmi and Zimmerman, 2005]:

$$\tau_{oct} = a + b\sigma_{m,2} \quad (3.25)$$

where τ_{oct} and $\sigma_{m,2}$ are defined in the equations (2.45) and (3.12). The constants a and b can be evaluated based on the Mohr-Coulomb parameters C_0 and q :

$$a = \frac{2\sqrt{2}}{3} \frac{C_0}{q+1} \quad (3.26)$$

$$b = \frac{2\sqrt{2}}{3} \frac{q-1}{q+1} \quad (3.27)$$

When $\sigma'_2 = \sigma'_3$ the criterion is identical to the Mohr-Coulomb failure criterion. Therefore Al-Ajmi and Zimmerman named the failure criterion Mogi-Coulomb.

3.6 Hoek-Brown

In 1980 Hoek and Brown proposed an empirical failure criterion in line with Mohr's hypothesis. The general form of this failure criterion is written [Martin et al., 1999]:

$$\sigma'_1 = \sigma'_3 + C_0 \left(m \frac{\sigma'_3}{C_0} + s \right)^a \quad (3.28)$$

where the constants m and s are empirical constants dependent on the rock mass quality. For large rock masses, such as underground formations, $a = 0.5$. For intact rock $s = 1$, which means that equation (3.28) can be simplified to:

$$\sigma'_1 = \sigma'_3 + \sqrt{mC_0\sigma_3 + C_0^2} \quad (3.29)$$

3.7 Griffith

The Griffith failure criterion, like the Mohr-Coulomb criterion, also neglects the intermediate principal stress. In the principal π -plane the cross-section of this failure criterion also becomes hexagonal, but this hexagon is regular. The original Griffith failure criterion follows:

$$(\sigma'_1 - \sigma'_3)^2 = 8T_0(\sigma'_1 + \sigma'_3) \quad \text{if } \sigma'_1 + 3\sigma'_3 > 0 \quad (3.30)$$

$$\sigma'_3 = -T_0 \quad \text{if } \sigma'_1 + 3\sigma'_3 < 0 \quad (3.31)$$

in the $\tau\sigma$ -plane the criterion is presented in the following form:

$$\tau^2 = 4T_0(\sigma + T_0) \quad (3.32)$$

The disadvantage with the Griffith failure criterion is that it is hard to fit to polyaxial tests since it is only dependent on a single variable. In 1963 Murrel extended the original Griffith failure criterion to account for the effect of the intermediate principal stress [Fjær et al., 2008]:

$$(\sigma'_1 - \sigma'_2)^2 + (\sigma'_1 - \sigma'_3)^2 + (\sigma'_2 - \sigma'_3)^2 = 24T_0(\sigma'_1 + \sigma'_2 + \sigma'_3) \quad (3.33)$$

This failure criterion is called the extended Griffith criterion. The cross-section in the π -plane is circular. The relation between uniaxial compressive strength and tensile strength is predicted by this criterion to be $C_0 = 12T_0$.

4 Drilling

In order to produce hydrocarbons from the sub surface one generally has to drill through underground formations of sedimentary rocks. Vertical stress, due to the overburden weight, and horizontal stresses, due to tectonic forces, will always act on an underground formation.

4.1 Stresses around a borehole

When drilling a well solid formation (which is under stress) is removed. This ultimately lead to a redistribution of the principal in situ stresses to maintain the rock mass in equilibrium. The principal stresses in formation mechanics are often assumed to be the vertical σ_v , minimum horizontal σ_h and maximum horizontal σ_H stress. The largest stress concentration for linear elastic materials occur at the borehole wall. Therefore borehole failure is expected to initiate at the borehole wall. Thus stresses around the borehole wall is essentially what needs to be compared against a failure criterion. [Al-Ajmi and Zimmerman, 2006]. Due to the cylindrical shape of a borehole it is necessary to express the stresses and strain in cylindrical coordinates. The most common approach for wellbore stability analysis is a linear poro-elasticity model [Rahimi et al., 2014]. The stresses at the borehole wall for nonporous materials, or nonporous materials with constant pore pressure, can be represented as:

$$\sigma_r = p_w \quad (4.1)$$

$$\sigma_\theta = \sigma_x^\circ + \sigma_y^\circ - 2(\sigma_x^\circ - \sigma_y^\circ) \cos 2\theta - 4\tau_{xy}^\circ \sin 2\theta - p_w \quad (4.2)$$

$$\sigma_z = \sigma_z^\circ - \nu_{fr}[2(\sigma_x^\circ - \sigma_y^\circ) \cos 2\theta + 4\tau_{xy}^\circ \sin 2\theta] \quad (4.3)$$

$$\tau_{r\theta} = \tau_{rz} = 0 \quad (4.4)$$

$$\tau_{\theta z} = 2(-4\tau_{xz}^\circ \sin \theta + 4\tau_{yz}^\circ \cos \theta) \quad (4.5)$$

where ν_{fr} is the Poisson's ratio of the formation. For a vertical well the

vertical principal stress σ_v is parallel to the z -axis. This simplifies the comparison between different failure criteria since all shear stresses disappear. The principal stresses can now be introduced and the stresses at the borehole wall can be expressed as [Fjær et al., 2008, p. 149]:

$$\sigma_r = p_w \quad (4.6)$$

$$\sigma_\theta = \sigma_H + \sigma_h - 2(\sigma_H - \sigma_h) \cos 2\theta - p_w \quad (4.7)$$

$$\sigma_z = \sigma_v - 2\nu_{fr}(\sigma_H - \sigma_h) \cos 2\theta \quad (4.8)$$

$$\tau_{r\theta} = \tau_{\theta z} = \tau_{rz} = 0 \quad (4.9)$$

where p_w is the internal wellbore pressure (mud pressure), ν is the Poisson ratio of the formation, σ_r is the radial-, σ_θ is the tangential- and σ_z is the vertical stress. Angle θ is measured relative to the axis of the maximum horizontal stress. From the equations (4.6)-(4.8) one can note that the axial and tangential stresses are functions of θ where both stresses reach a maximum value at $\theta = \pm\pi/2$ and a minimum value at $\theta = 0$ or π [Al-Ajmi and Zimmerman, 2006]. Therefore mechanical failure will only occur at these points. Furthermore these equations state that it's only the radial and tangential stresses that depend on the mud pressure, hence these are the stresses affecting wellbore stability. As previously mentioned the two main wellbore stability issues related to drilling are: shear failure in the form of breakout formation leading to borehole collapse and tensile failure in form of hydraulic fracturing. These issues are associated to the radial and tangential stresses in such way that when $\sigma_r \geq \sigma_\theta$ fracture occurs, and when $\sigma_\theta \geq \sigma_r$ collapse occurs.

Wellbore stability issues can be avoided if the maximum allowable mud pressure p_{wf} and the minimum allowable mud pressure p_{wb} are predicted correctly. For hydraulic fracturing there are three different stress states that are in alignment with $\sigma_r \geq \sigma_\theta$. These are: $\sigma_r \geq \sigma_\theta \geq \sigma_z$, $\sigma_r \geq \sigma_z \geq \sigma_\theta$ and $\sigma_z \geq \sigma_r \geq \sigma_\theta$, which have to be investigated in order to determine p_{wf} . When p_w increases, σ_θ decreases towards the tensile strength of the rock which will

first be exceeded where the tangential stress will have the lowest value ($\theta = 0$ or π). This is the same direction as the principal axis of $\sigma - H$, hence the three principal stresses at the borehole wall are [Al-Ajmi and Zimmerman, 2006]:

$$\sigma_r = p_w \quad (4.10)$$

$$\sigma_\theta = 3\sigma_h - \sigma_H - p_w \quad (4.11)$$

$$\sigma_z = \sigma_v - 2\nu_{fr}(\sigma_H - \sigma_h) \quad (4.12)$$

Similarly the stress states in alignment with collapse, and thus $\sigma_\theta \geq \sigma_r$, are found. $\sigma_z \geq \sigma_\theta \geq \sigma_r$, $\sigma_\theta \geq \sigma_z \geq \sigma_r$ and $\sigma_\theta \geq \sigma_r \geq \sigma_z$. The compressive strength of the rock will be first exceeded at the directions where σ_z and σ_θ reaches their maximum value. As previously mentioned this happens when $\theta = \pm\pi/2$. Consequently the principal stresses at the borehole wall become:

$$\sigma_r = p_w \quad (4.13)$$

$$\sigma_\theta = 3\sigma_H - \sigma_h - p_w \quad (4.14)$$

$$\sigma_z = \sigma_v + 2\nu_{fr}(\sigma_H - \sigma_h) \quad (4.15)$$

4.2 Mohr-Coulomb borehole failure

To find the critical mud pressures one has to make use of a failure criterion. For every case that will lead to fracture, equations (4.10)-(4.12) will have to be inserted into equation (3.8) in the right manor. In example $\sigma_r \geq \sigma_\theta \geq \sigma_z$ will lead to:

$$p_w = C + q[\sigma_v - 2\nu_{fr}(\sigma_H - \sigma_h)] \quad (4.16)$$

$p_w=p_{wf1}$ which is the maximum allowable mud pressure for this first investi-

gated stress state. If this mud pressure is exceeded hydraulic fracturing will occur for this case.

All three stress states for hydraulic fracturing, and the three stress states for collapse, are investigated in the same manor (see table 1 and 2).

The same procedure goes for all wellbore stability analysis. First a constitutive model of the well bore stresses at the borehole wall is chosen. Second one defines the cases for fracturing and collapse and include the principal stresses in a chosen failure criteria. Solving for p_w yields the critical pressures.

$\sigma_1 \geq \sigma_2 \geq \sigma_3$	Hydraulic fracturing when $p_w \geq p_{wf}$
$\sigma_r \geq \sigma_\theta \geq \sigma_z$	$p_{wf1} = C + q[\sigma_v - 2v_{fr}(\sigma_H - \sigma_h)]$
$\sigma_r \geq \sigma_z \geq \sigma_\theta$	$p_{wf2} = \frac{C+q(3\sigma_h-\sigma_H)}{1+q}$
$\sigma_z \geq \sigma_r \geq \sigma_\theta$	$p_{wf3} = \frac{C-(\sigma_v-2v_{fr}(\sigma_H-\sigma_h))}{q+(3\sigma_h-\sigma_H)}$

Table 1: Mohr-Coulomb criterion for fracture pressure in vertical wellbores.

$\sigma_1 \geq \sigma_2 \geq \sigma_3$	Formation breakout when $p_w \leq p_{wb}$
$\sigma_z \geq \sigma_\theta \geq \sigma_r$	$p_{wb1} = \frac{[\sigma_v+2v_{fr}(\sigma_H-\sigma_h)]-C}{q}$
$\sigma_\theta \geq \sigma_z \geq \sigma_r$	$p_{wb2} = \frac{(3\sigma_H-\sigma_h)-C}{1+q}$
$\sigma_\theta \geq \sigma_r \geq \sigma_z$	$p_{wb3} = (3\sigma_H - \sigma_h) - C - q[\sigma_v + 2v_{fr}(\sigma_H - \sigma_h)]$

Table 2: Mohr-Coulomb criterion for collapse pressure in vertical wellbores.

5 Method

5.1 PSI simulations

To compare the four failure criteria Mohr-Coulomb, Drucker-Prager, Modified Lade and Stassi-D'Alia a software called PSI v5.22s provided by SINTEF Research Petroleum has been used. PSI takes in three major types of data inputs; wellbore conditions, formation conditions, formation properties and estimates the mechanical stability of the wellbore. Default values have been set for all required parameters to help the user simulate results even with limited data.

Results are presented in a mud-weight window where the window itself is defined as the range of mud-weights where the probabilities for shear- or tensile failure are both estimated to be less than 0.5 around the wellbore. Alternatively the window is defined by the probability for collapse and mud loss being equal to 0.5. The failure probability is estimated around the whole wellbore at the given depth of interest.

The different cases that the author has assumed for investigating the different failure criteria's response to deviation are listed in the following sub-chapters. Regarding the formation properties and the mud properties default values, or rough assumptions, has mainly been used.

5.1.1 Case 1: Weak shale

The first case used to compare the different failure criteria describes a vertical well moments after it has been drilled through a weak shale (North Sea) formation. The strength properties are extracted from table C1. At the measured depth of investigation the following wellbore conditions, formation conditions and formation properties are assumed and used:

Wellbore conditions				
T [C°]	d [inch]	t [days]	Inc [$^\circ$]	D [m]
60.0	12.25	10^{-3}	0	1850

Formation conditions				
σ_v [MPa]	σ_h [MPa]	σ_H [MPa]	p_p [MPa]	T_f [C°]
38.1	34.5	37.0	31.2	80.0

Formation properties						
C_0 [MPa]	φ [$^\circ$]	T_0 [MPa]	E [GPa]	v_{fr} []	Φ [%]	k [nD]
6.0	20.0	0.242	4.01	0.354	9.7	10.0

Table 3: Inputs for case 1 where T is wellbore temperature, t is time since drilling, d is wellbore diameter, D is depth of investigation, T_f is formation temperature, p_p is the in situ pore pressure, φ is the angle of internal friction, Φ is the porosity and k is the permeability

5.1.2 Case 2a: Triassic shale

The same approach as in case 1 has been used for case 2a. The different failure criteria compared for a vertical well moments after drillout in case 2a is presented as a dashed line in case 2b and 2c. In this part the failure criteria's sensibility for inclination and azimuth are compared. Strength properties for this case have been extracted from [Horsrud et al., 1998] and the chosen shale type is from the Triassic geological time period at a depth of 2500 meters. The input values that have been modified for this investigation is shown in the table below:

Wellbore conditions						
T [C°]	d [inch]	t [days]	Inc [$^\circ$]	D [m]		
60.0	12.25	10^{-3}	0	2500		
Formation conditions						
σ_v [MPa]	σ_h [MPa]	σ_H [MPa]	p_p [MPa]	T_f [C°]		
50.0	40.0	45.0	30.0	100.0		
Formation properties						
C_0 [MPa]	φ [$^\circ$]	T_0 [MPa]	E [GPa]	v_{fr} []	Φ [%]	k [nD]
13.0	14.9	0.242	2.0	0.17	15.0	22.0

Table 4: Inputs for case 2a

5.1.3 Case 2b and 2c

Case 2b and 2c assumes the same wellbore conditions and formation properties as in case 2a (table 4). However case 2b and 2c assume isotropic horizontal stresses given in the table below:

Formation conditions 2b			
σ_v [MPa]	σ_h [MPa]	σ_H [MPa]	p_p [MPa]
50.0	40.0	40.0	30.0

Formation conditions 2c			
σ_v [MPa]	σ_h [MPa]	σ_H [MPa]	p_p [MPa]
50.0	45.0	45.0	30.0

Table 5: Formation conditions for case 2b and 2c

5.2 Matlab calculations

Matlab has also been used in order to compute the critical collapse pressure (i.e. lower limit of mud window) for the Mohr-Coulomb and the Mogi-Coulomb failure criteria.

In order to determine if a wellbore is mechanically instable one must first model the stresses around it. When a well is drilled the principal in-situ stresses will be altered which leads to a stress concentration around the wellbore. The largest stress concentration will occur at the wellbore wall for a linear elastic material. Therefore failure will initiate here. Once the wellbore wall stresses are found they are compared against a failure criterion. As previously mentioned, a failure criterion is simply an empirical model of the strength of the rock. [Al-Ajmi and Zimmerman, 2006].

In the following section the theory behind a suggested Matlab script is provided. Function codes written by the author is provided in Appendix B. The author has focused on providing an output of the calculations that are graphically easy to interpret with respect to the optimal deviation according to collapse pressure for the selected failure criterion.

The first step is to arrange the principal far field stresses into a stress tensor. Often it is assumed that the principal stresses in a formation equals the far field stresses σ_v , σ_H and σ_h . This is not always true. Therefore one has to transform the principal stress tensor into a coordinate system that is easy to refer to. To organize the in-situ far field principal stresses into a geographical coordinate system where north, east and downward (parallel to gravity) are the coordinate axes one can use a rotation matrix

$$\mathbf{R}_G = \begin{pmatrix} \cos \alpha \cos \beta & \sin \alpha \cos \beta & -\sin \beta \\ \cos \alpha \sin \beta \sin \gamma - \sin \alpha \cos \gamma & \sin \alpha \sin \beta \sin \gamma + \cos \alpha \cos \gamma & \cos \beta \sin \gamma \\ \cos \alpha \sin \beta \cos \gamma + \sin \alpha \sin \gamma & \sin \alpha \sin \beta \cos \gamma - \cos \alpha \sin \gamma & \cos \beta \cos \gamma \end{pmatrix} \quad (5.1)$$

where γ, β and α are the rotation angles (see chapter 2.1.1). However when

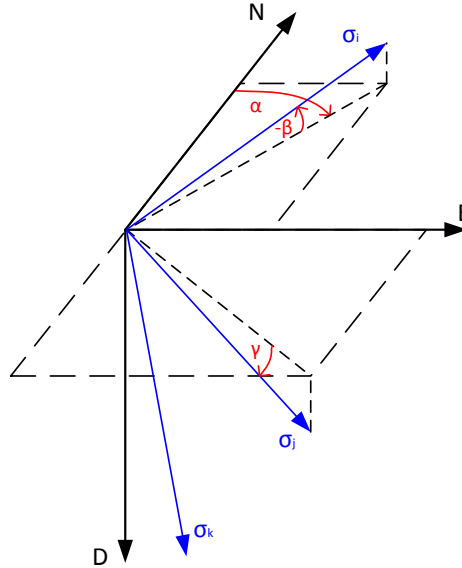


Figure 13: Angle relationship between a principal stress coordinate system and the geographical coordinate system.

not knowing the direction in which the far-field principal stresses are acting it is fair to assume that the vertical stress is acting parallel to gravity, thus $\beta = \gamma = 0$. \mathbf{R}_G , the geographical rotation matrix, transforms known far-field in-situ principal stresses into a geographic stress tensor through

$$\boldsymbol{\sigma}_G = \mathbf{R}_G^T \boldsymbol{\sigma}_P \mathbf{R}_G \quad (5.2)$$

where \mathbf{R}_G^T is the transpose matrix of \mathbf{R}_G . $\boldsymbol{\sigma}_G$ describes the far field in-situ stresses in a geographical Cartesian coordinate system. The matlab code for this step is provided in section B.1.2. For a deviated wellbore one has to transform the tensor $\boldsymbol{\sigma}_G$ again so it refers to the wellbore's inclination and azimuth.

From figure 14 a rotation matrix can be developed.

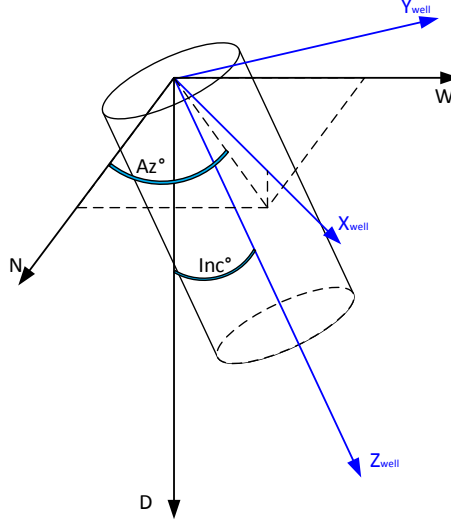


Figure 14: Angle relationship between the geographical coordinate system and a wellbore coordinate system.

$$\mathbf{R}_B = \begin{pmatrix} \cos(Az^\circ) \cos(Inc^\circ) & \sin(Az^\circ) \cos(Inc^\circ) & -\sin(Inc^\circ) \\ -\sin(Az^\circ) & -\cos(Az^\circ) & 0 \\ \cos(Az^\circ) \sin(Inc^\circ) & \sin(Az^\circ) \sin(Inc^\circ) & \cos(Inc^\circ) \end{pmatrix} \quad (5.3)$$

The rotation matrix \mathbf{R}_B can then transform the geographical stress tensor, $\boldsymbol{\sigma}_G$, into a wellbore stress tensor through the transformation formula:

$$\boldsymbol{\sigma}_B = \mathbf{R}_B \boldsymbol{\sigma}_G \mathbf{R}_B^T \quad (5.4)$$

The matlab code for this step is provided in appendix B.1.3. The stresses on the wellbore wall can then be found from Kirsch equations [Fjær et al., 2008]. For investigation of failure initiation at the wellbore wall, one has to insert the state of stress into a failure criterion. Therefore it is convenient to express the stresses as effective stresses. Thus the Kirsch equations at the

wellbore wall can be written (for the general solution formula see appendix B.2.1):

$$\sigma'_r = p_w - p_p \quad (5.5)$$

$$\sigma'_\theta = \sigma_{Bx} + \sigma_{By} - 2(\sigma_{Bx} - \sigma_{By}) \cos 2\theta - 4\tau_{Bxy} \sin 2\theta - p_w - p_p \quad (5.6)$$

$$\sigma'_z = \sigma_{Bz} - \nu_{fr} [2(\sigma_{Bx} - \sigma_{By}) \cos 2\theta + 4\tau_{Bxy} \sin 2\theta] - p_p \quad (5.7)$$

$$\tau_{r\theta} = \tau_{rz} = 0 \quad (5.8)$$

$$\tau_{\theta z} = 2(-\tau_{Bxz} \sin \theta + \tau_{Byz} \cos \theta) \quad (5.9)$$

From equation (5.5) - (5.6) it is clear that the stresses at the wellbore wall varies with θ , the position around the wellbore. To find the principal wellbore wall stresses as described in equation (2.20) the formula becomes (appendix B.2.2):

$$\sigma'_{1,2} = \frac{\sigma'_\theta + \sigma'_z}{2} \pm \frac{\sqrt{(\sigma'_\theta - \sigma'_z)^2 + 4\tau_{\theta z}^2}}{2} \quad (5.10)$$

Depending on the magnitude of σ'_r the principal stress subscripts can be organized so that it matches the magnitude of the principal effective stresses. From equation (5.10) one can note that the only possibilities are:

$$\sigma'_1 \geq \sigma'_2 \geq \sigma'_r, \sigma'_1 \geq \sigma'_r \geq \sigma'_2 \text{ and } \sigma'_r \geq \sigma'_1 \geq \sigma'_2$$

For wellbore shear failure, where breakouts are the result, it is often σ'_r that equals σ'_3 . To find the minimum wellbore pressure required to avoid failure initiation the principal stresses are inserted to a failure criterion of choice. Mohr-Coulomb failure criterion generates the following equation:

$$\frac{\sigma'_\theta + \sigma'_z}{2} + \frac{\sqrt{(\sigma'_\theta - \sigma'_z)^2 + 4\tau_{\theta z}^2}}{2} = C_0 + \tan^2 \beta (p_w - p_p) \quad (5.11)$$

Both σ'_r and σ'_θ depends on p_w and so to solve for p_w it is necessary to extend equation (5.11) further:

$$\frac{A - p_w}{2} + \frac{\sqrt{(B - p_w)^2 + C}}{2} = C_0 + \tan^2 \beta (p_w - p_p) \quad (5.12)$$

where (appendix B.3.1):

$$A = \sigma_{Bx} + \sigma_{By} - 2(\sigma_{Bx} - \sigma_{By}) \cos 2\theta - 4\tau_{Bxy} \sin 2\theta - p_p + \sigma'_z \quad (5.13)$$

$$B = \sigma_{Bx} + \sigma_{By} - 2(\sigma_{Bx} - \sigma_{By}) \cos 2\theta - 4\tau_{Bxy} \sin 2\theta - p_p - \sigma'_z \quad (5.14)$$

$$C = 4\tau_{\theta z}^2 \quad (5.15)$$

The complexity of equation (5.12) requires a numerical approach when solving for p_w . By creating a function of equation (5.12) that equals zero, where p_w is the only variable, the Newton–Raphson method can be used to solve for p_w :

$$f(p_w) = A - 2C_0 + Dp_p + \sqrt{(B - p_w)^2 + C} - p_w(1 + D) = 0 \quad (5.16)$$

$$f'(p_w) = \frac{p_w - B}{\sqrt{(B - p_w)^2 + C}} - D - 1 \quad (5.17)$$

$$D = 2 \tan^2 \beta \quad (5.18)$$

This requires that the first derivative of the function is provided. Other failure criteria, where the intermediate principal stress is considered, yield more complex functions. Finding the derivative of these functions will be more time consuming than for the Mohr-Coulomb failure criterion. In that case another numerical approach will be necessary to use in order to solve for then minimum required mud pressure. The bisection method has been preferred by the author (appendix B.3.4). For the Mogi-Coulomb failure criterion the following function was derived:

$$\begin{aligned}
f(p_w) = & \\
& \frac{1}{3} \left[(B - p_w)^2 + C + \left(\frac{A - p_w}{2} - \frac{\sqrt{(B - p_w)^2 + C}}{2} - p_w + p_p \right)^2 \right. \\
& \left. + \left(p_w - p_p - \frac{A - p_w}{2} - \frac{\sqrt{(B - p_w)^2 + C}}{2} \right)^2 \right]^{\frac{1}{2}} \\
& - a - b \frac{\left(\frac{A - p_w}{2} + \frac{\sqrt{(B - p_w)^2 + C}}{2} + p_w - p_p \right)}{2} = 0
\end{aligned} \tag{5.19}$$

where a and b are defined in the equations (3.26) and (3.27) (appendix B.3.3). In order to present the required mud pressures for inclinations between 0° and 90° for all possible directions the procedure described above is performed in iterative loops for all values of θ , azimuth and inclination. The final output is plotted in a disc-plot (fig. 15). The main script is shown in appendix B.4:

6 Results

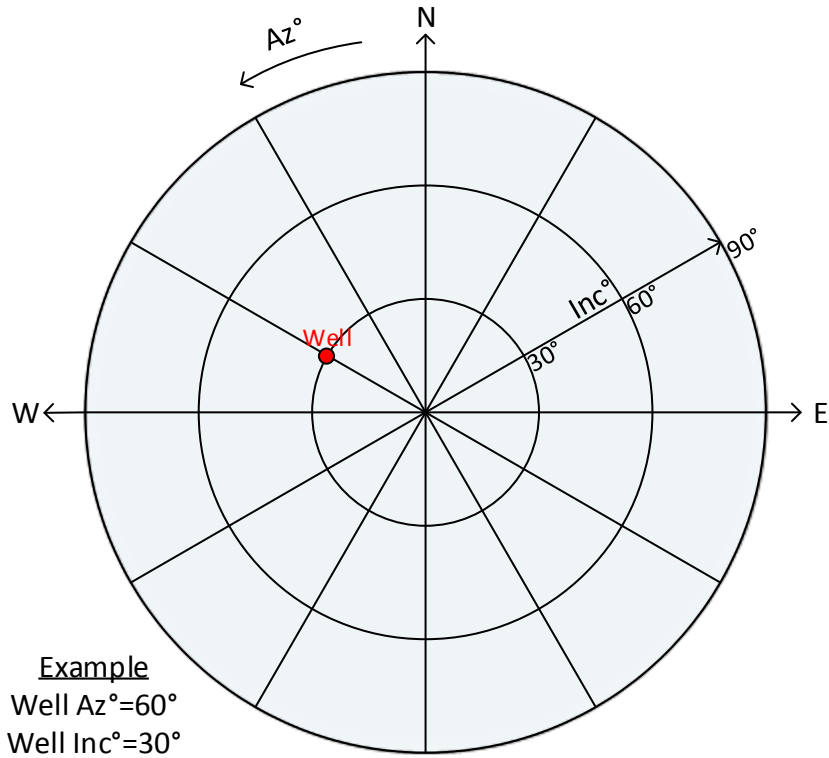


Figure 15: A disc plot graphically presenting the most beneficial inclination with respect to collapse pressure for a given failure criteria.

6.1 Comparing failure criteria in PSI case 1

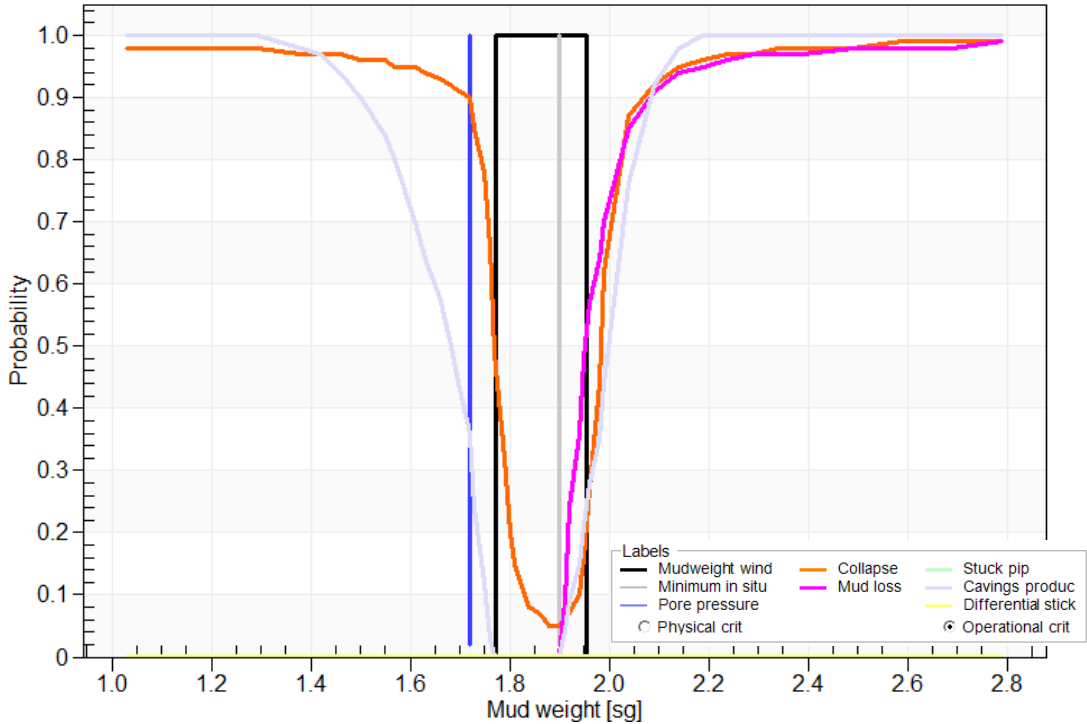


Figure 16: Mud weight window analysis for case 1 using the Mohr-Coulomb failure criterion.

Figure 16 reveals a very narrow mud-weight window when using the Mohr-Coulomb failure criterion for case 1. This result coincides with the theory and historical observations saying that the Mohr-Coulomb failure criterion conservatively over estimates the required mud weight for collapse. According to this result there is a 50% probability for failure for an equivalent mud weight of 1.77 sg. Using the Mohr-Coulomb failure criterion clearly excludes the possibility for under balanced drilling when the probability for failure at the pore pressure line (1.72 sg) is 90%. Conventional drilling risks the usage of an unnecessary high mud weight that will decrease the rate of penetration. The probability for mud loss rapidly increases from zero when the equivalent mud weight starts to exceed the minimum in situ stress σ_h .

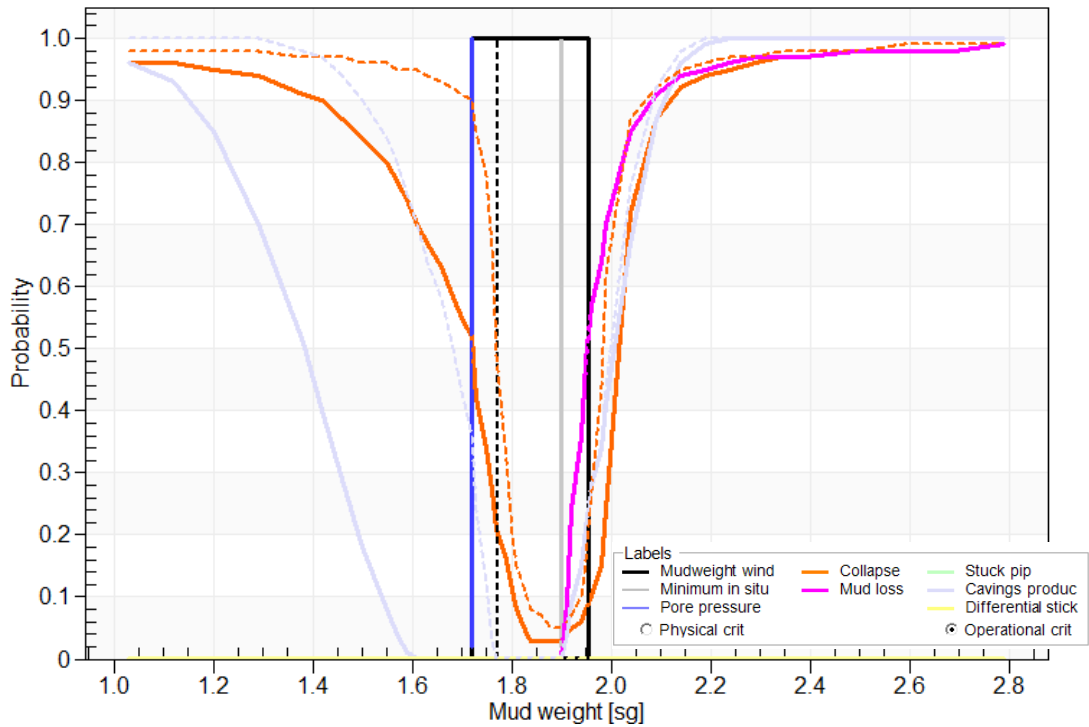


Figure 18: Mud weight window analysis for case 1 comparing the Modified Lade failure criterion with the Mohr-Coulomb failure criterion (dashed).

The Modified Lade criterion also predicts the same probability for mud loss as the Mohr-Coulomb failure criterion. The lower mud-weight limit is lower than for Mohr-Coulomb failure criterion prediction, but higher than for the Drucker-Prager failure criterion prediction and now exactly equal to the pore pressure (1.72 sg). For the lower mud weight limit of the Mohr-Coulomb failure criterion Modified Lade predicts a 20% probability for collapse. However the Modified Lade criterion does not suggest any possibilities for under balanced drilling. If the mud weight is kept between the pore pressure and minimum in situ stress there are no possibility for cavings production. Appendix A.1 contains a plot that compares Drucker-Prager and the Modified Lade criterion. There it is seen that the Modified Lade criterion predicts a higher lower mud weight limit than the Drucker-Prager failure criterion.

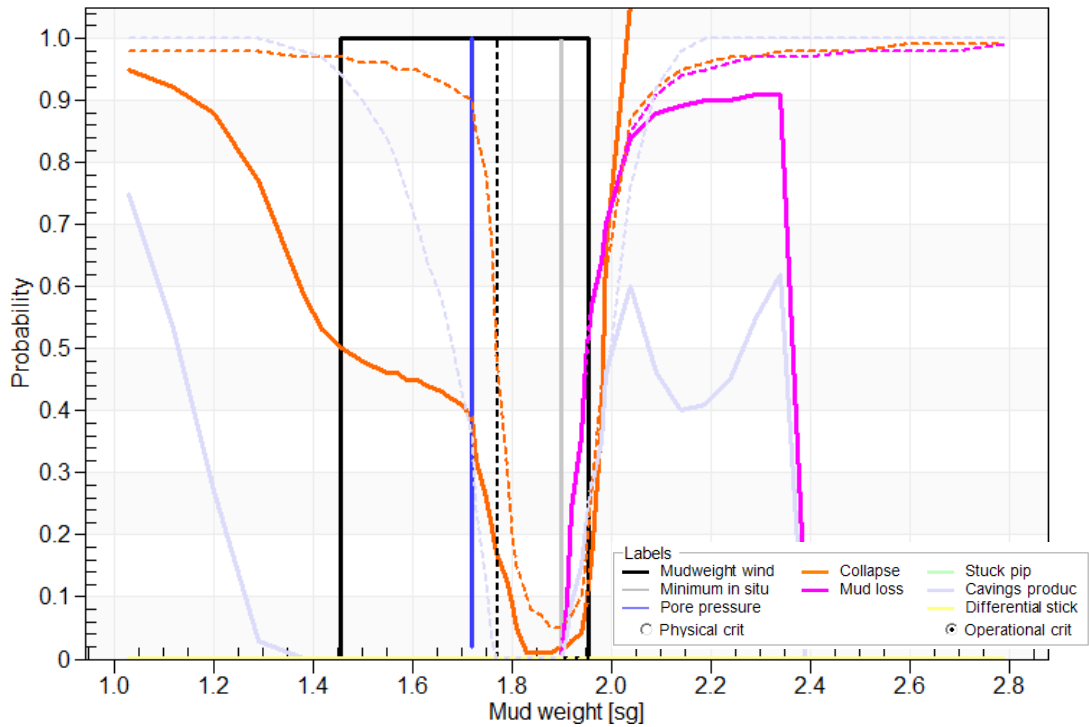


Figure 19: Mud weight window analysis for case 1 comparing the simplified Stassi-D’Alia failure criterion with the Mohr-Coulomb failure criterion (dashed).

The simplified Stassi-D’Alia criterion predicts the lowest lower mud-weight limit out of the four failure criteria for case 1. The estimated equivalent mud-weight value for 50% probability for collapse is 1.45 sg. Figure 19 compares the Stassi-D’Alia failure criterion with the Mohr-Coulomb failure criterion but in appendix A.1 one can clearly see that the Stassi-D’Alia failure criterion predicts the same probability for collapse (40%), when the mud-weight equals the in situ pore pressure (1.72 sg), as the Drucker-Prager failure criterion does. The Stassi-D’Alia failure criteria assumes the same probability for mud loss as the other failure criteria within the mud weight window.

6.1.1 Inclination sensibility case 1

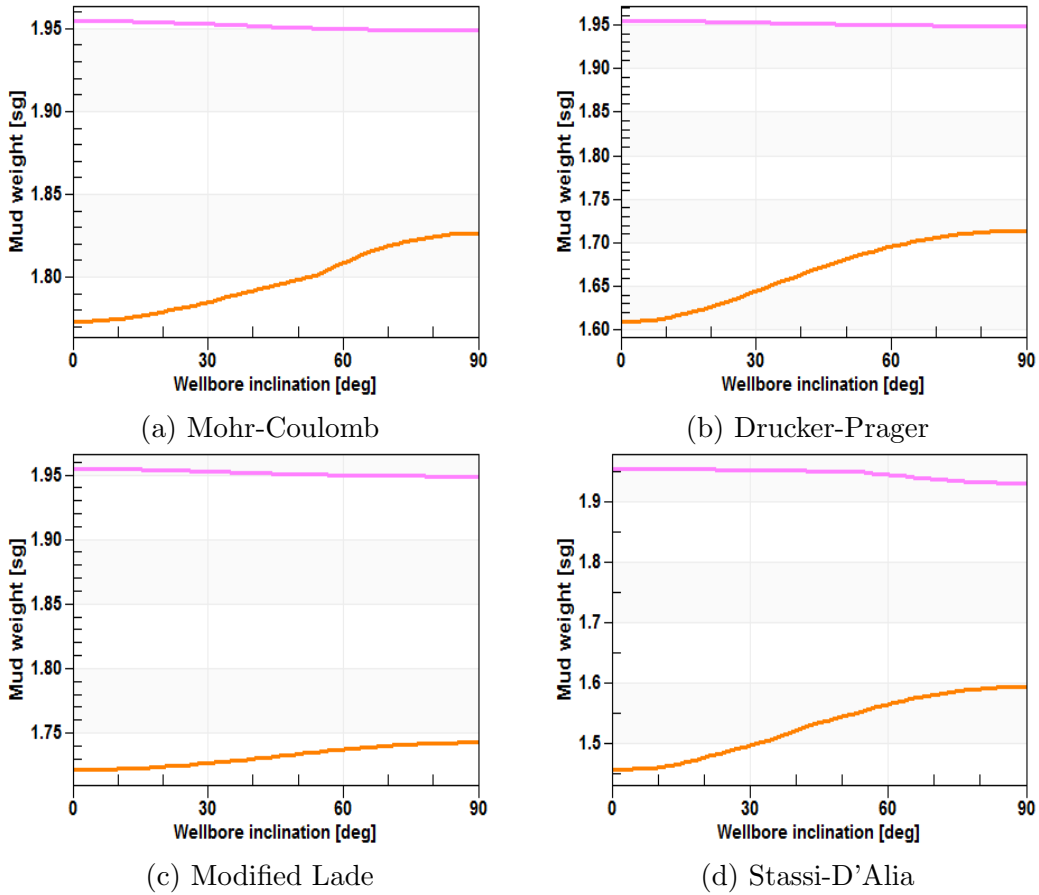


Figure 20: Comparing the four different failure criteria's inclination sensibility regarding the mud weight window for well trajectories along the maximum horizontal in situ stress direction.

For an inclined wellbore trajectory in the maximum horizontal in situ stress direction the mud loss limit decreases insignificantly for all four failure criteria in case 1. At 90° inclination only the Stassi-D'Alia failure criterion predicts a marginally lower limit (≈ 1.925 sg) than the other criteria (1.95 sg) where the probability for mud loss is 50%. According to figure 20 it is fair to assume that the choice of failure criteria is not critical for evaluating the probability for mud loss in this direction.

The collapse pressure increases for all four failure criteria with a similar trend. The Modified Lade failure criterion is the least inclination sensitive failure criteria for case 1 in the given direction. At 90° inclination the Stassi-D'Alia failure criterion predicts an equivalent collapse pressure of 1.60 sg which is lower than the equivalent collapse pressure at 0° inclination for all the other failure criteria. For case 1 the choice of failure criteria is critical to properly evaluate the collapse pressure.

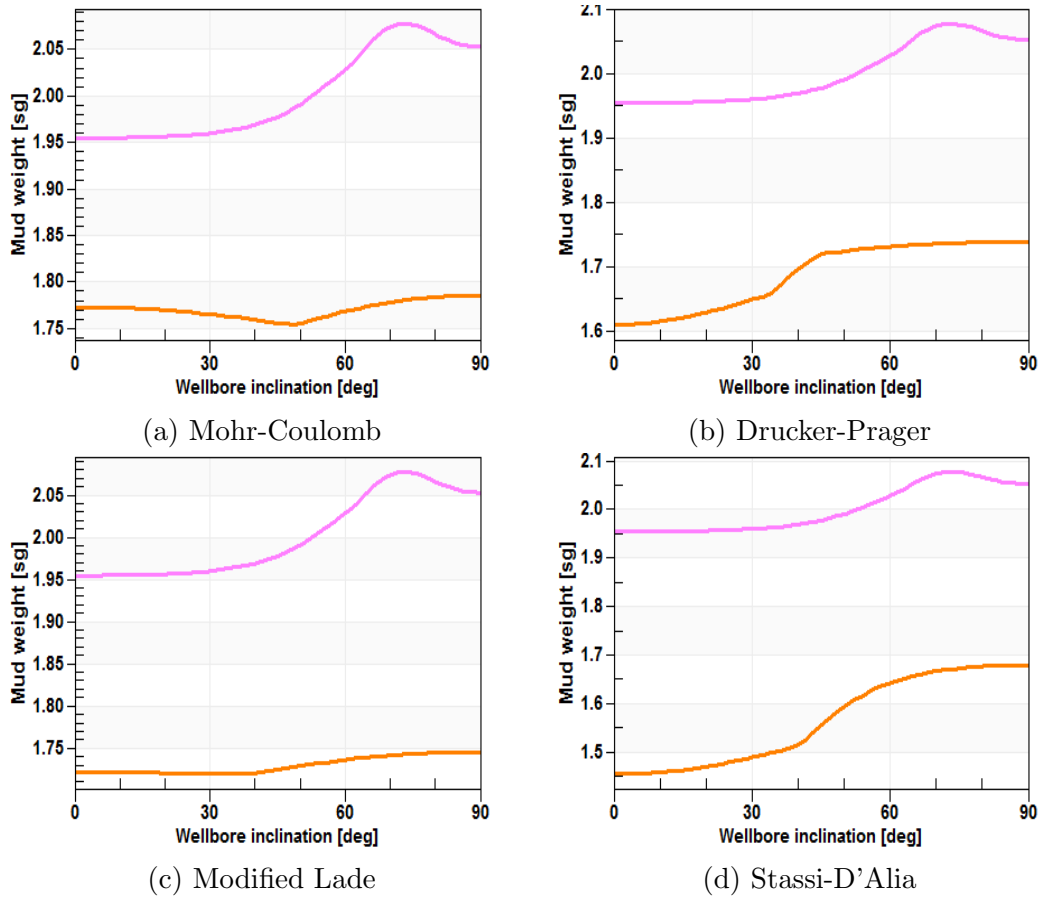


Figure 21: Comparing the four different failure criteria's inclination sensibility regarding the mud weight window for well trajectories along the minimum horizontal in situ stress direction.

For an inclined wellbore trajectory in the minimum horizontal in situ stress direction the mud loss limit behaves the same for all four failure criteria. In this direction the risk of mud loss decreases from $\approx 30^\circ$ inclination. An inclined wellbore in this direction is therefore beneficial for case 1. Also it is fair to say that the choice of failure criteria is not critical concerning mud loss in case 1.

For the evaluation of collapse pressure inclination sensibility in the direction of the minimum horizontal stress the different failure criteria provides varying predictions. The collapse pressure for the Modified Lade failure criterion is approximately the same in figure 21c as in figure 20c. The Mohr-Coulomb failure criterion clearly states that for case 1 it is beneficial to drill in the direction of the minimum horizontal in situ stress with respect to collapse, and if possible one should do so with a wellbore inclination of $\approx 50^\circ$. At 90° inclination the Stassi-D'Alia failure criterion predicts the lowest collapse probability followed by Drucker-Prager and Modified Lade failure criteria.

6.1.2 Azimuth sensibility for case 1

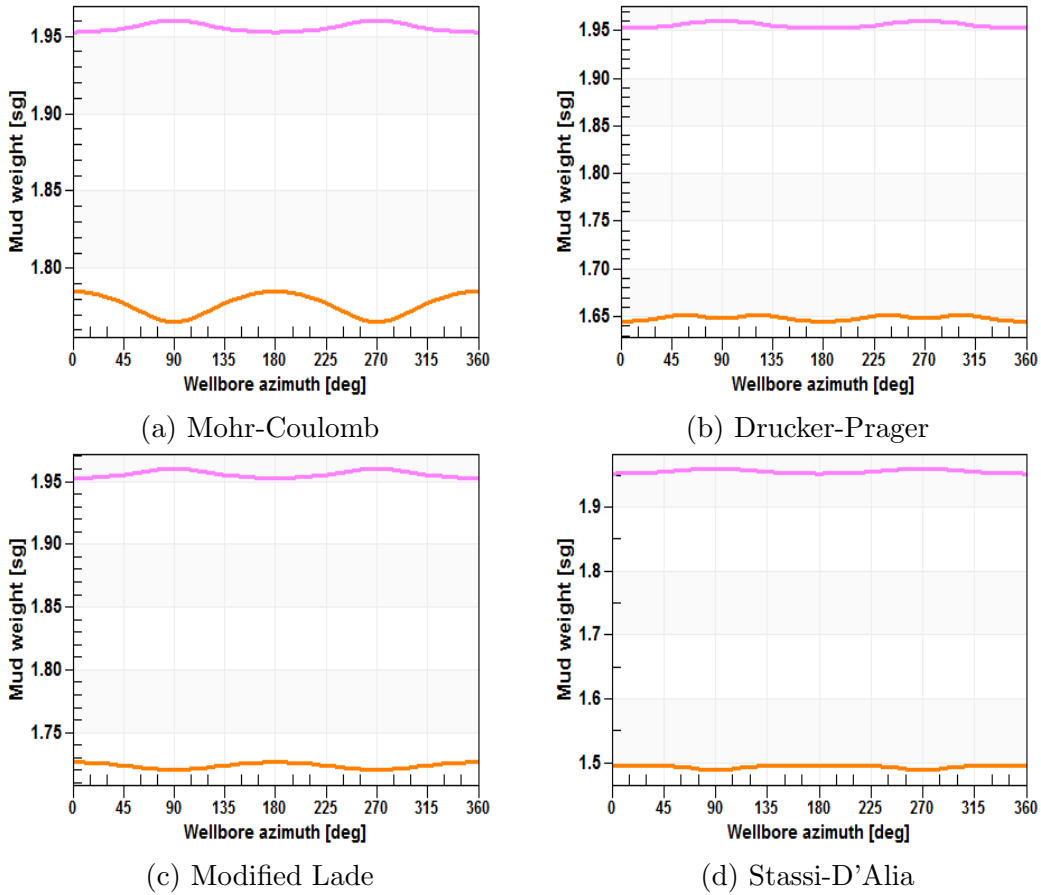


Figure 22: Comparing the four different failure criteria's azimuth sensibility regarding the mud weight window for a 30° inclined wellbore.

For a 30° inclined wellbore the Mohr-Coulomb criterion is the only failure criterion that clearly states a preferred wellbore azimuth with respect to collapse pressure. Still it predicts the highest collapse pressure for all azimuths. According to figure 22a the optimal azimuth regarding both collapse and mud loss is in the direction of the minimum in situ stress. This result coincide with figure 21a and figure 20a. The other failure criteria show marginally fluctuations and it seems like the mud loss pressure behaves similarly for all four criteria. This coincide with the results provided in figure 16 - 19. The Stassi-D'Alia failure criterion consistently predicts the lowest collapse pressure for all azimuths.

6.1 Comparing failure criteria in PSI case 1

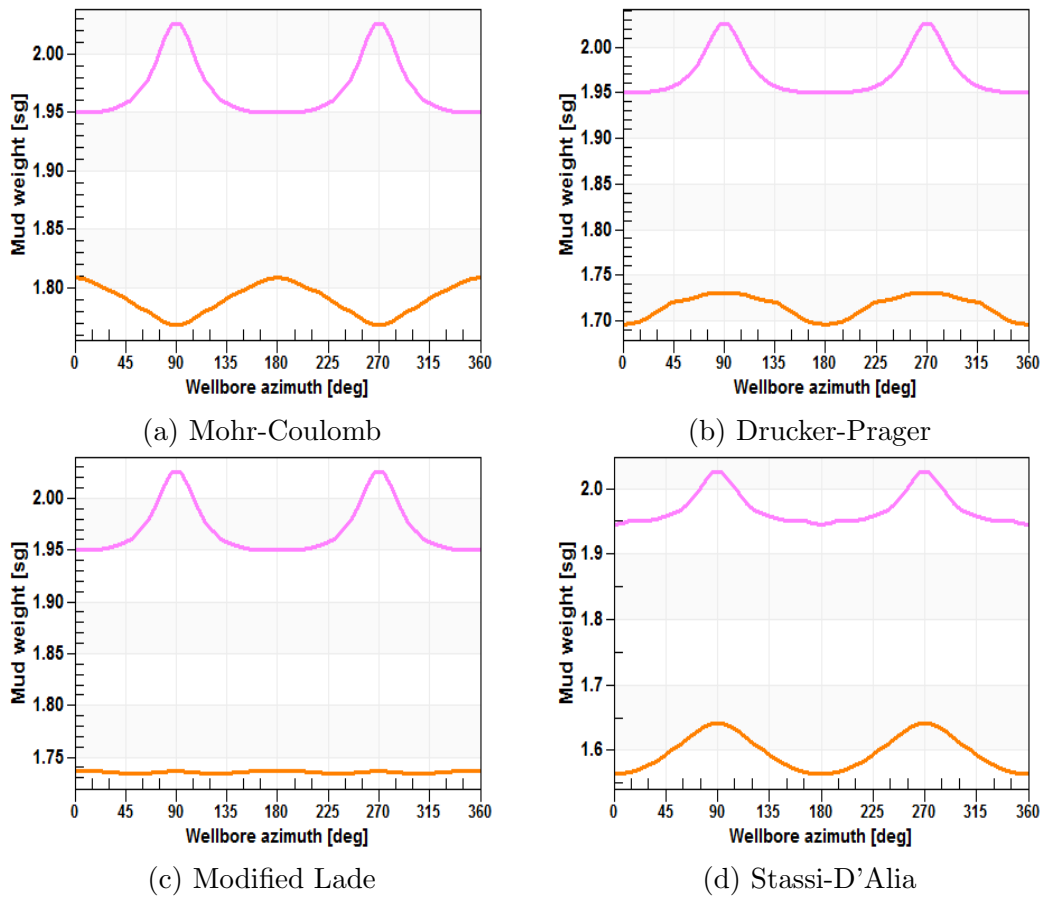


Figure 23: Comparing the four different failure criteria's azimuth sensibility regarding the mud weight window for a 60° inclined wellbore.

For a 60° inclined wellbore all the failure criteria give approximately the same result for mud loss pressure. This follows the previously presented results. The Modified Lade failure criterion predicts roughly the same collapse pressure as in figure 22c. For all the previous presented sensibility results the Modified Lade failure criterion shows little sensibility for both azimuth and inclination when it comes to predicting the collapse pressure.

It is interesting to note that the Mohr-Coulomb failure criterion predicts the direction of the minimum horizontal in situ stress as the most beneficial azimuth regarding collapse pressure, whereas the Drucker-Prager and Stassi-D'Alia failure criteria states the opposite for a 60° inclined wellbore. However the Stassi-D'Alia failure criterion still predicts the lowest collapse pressure followed by the Drucker-Prager failure criterion.

6.2 Matlab results case 1

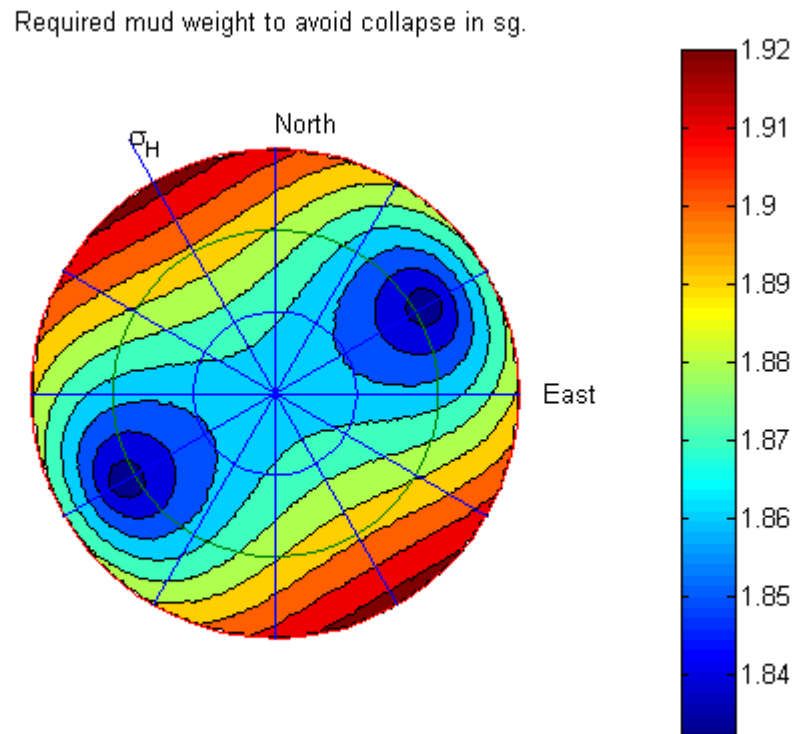


Figure 24: Minimum required mud weight to avoid collapse failure initiation in case 1 for the Mohr-Coulomb failure criterion according to the Matlab calculations.

Figure 24 generally coincide with the sensibility analyses previously performed for case 1. The required mud weight is higher due to the fact that the Matlab program assumes a perfect brittle failure as soon as the requirement for failure is reached whereas the PSI simulations consider plasticity and other factors which only produce a slight possibility for failure at the time the Matlab program predicts failure

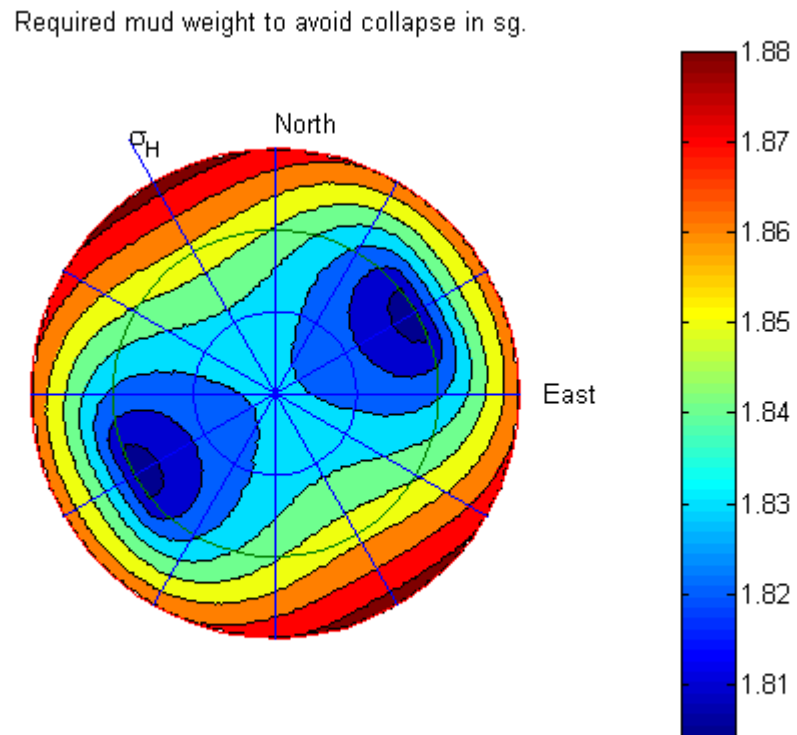


Figure 25: Minimum required mud weight to avoid collapse failure initiation in case 1 for the Mogi-Coulomb failure criterion according to the Matlab calculations.

Figure 25 shows that the Mogi-Coulomb failure criterion prefers the same deviation as the Mohr-Coulomb failure criterion. The Mogi-Coulomb failure criterion predicts a slightly lower required mud weight to avoid collapse which coincide with the theory.

6.3 Case 2a

6.3.1 Inclination sensibility case 2a

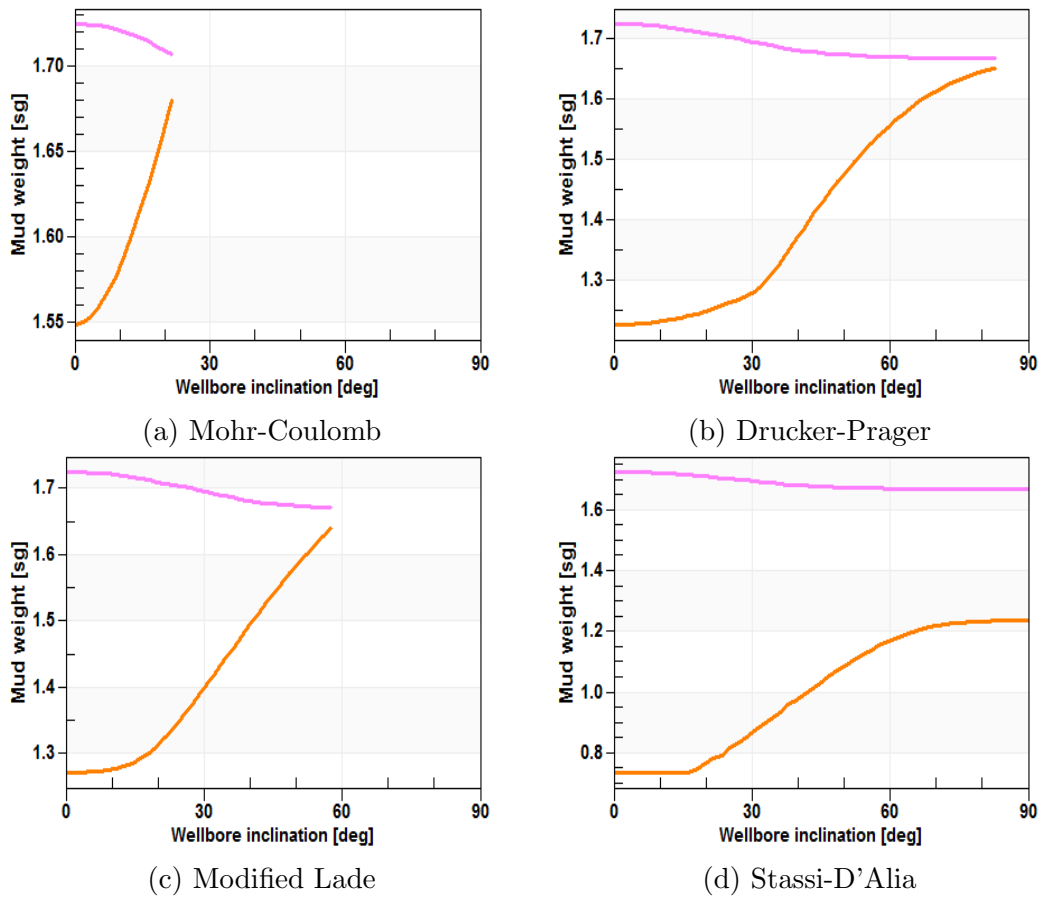


Figure 26: Comparing the four different failure criteria's inclination sensibility in case 2a regarding the mud weight window for well trajectories along the maximum horizontal in situ stress direction.

As in case 1 the failure criteria are consistent when predicting the mud loss pressure in case 2a. When it comes to collapse pressure however, a wide variety is shown in figure 26. Figure 26a show that when drilling along the maximum horizontal in situ stress direction the Mohr-Coulomb failure criterion predicts that one can only deviate the wellbore 20° . Figure 26b states that the Drucker-Prager failure criterion predicts no major operational limitations compared to a vertical well for inclinations up to 30° . When the inclination increases above 30° the collapse pressure rapidly increases and at 80° inclination the mud-weight window is too narrow. For the Modified Lade failure criterion (fig. 26c) we see the same collapse pressure development for increasing inclination as for the Drucker-Prager failure criterion. Although the Modified Lade failure criterion predicts a maximum possible inclination in this direction to be approximately 55° . The Stassi-D'Alia failure criterion is the only failure criterion that predicts the possibility for a 90° inclined wellbore in this direction. Also the mud weight window is reasonably wide at this inclination.

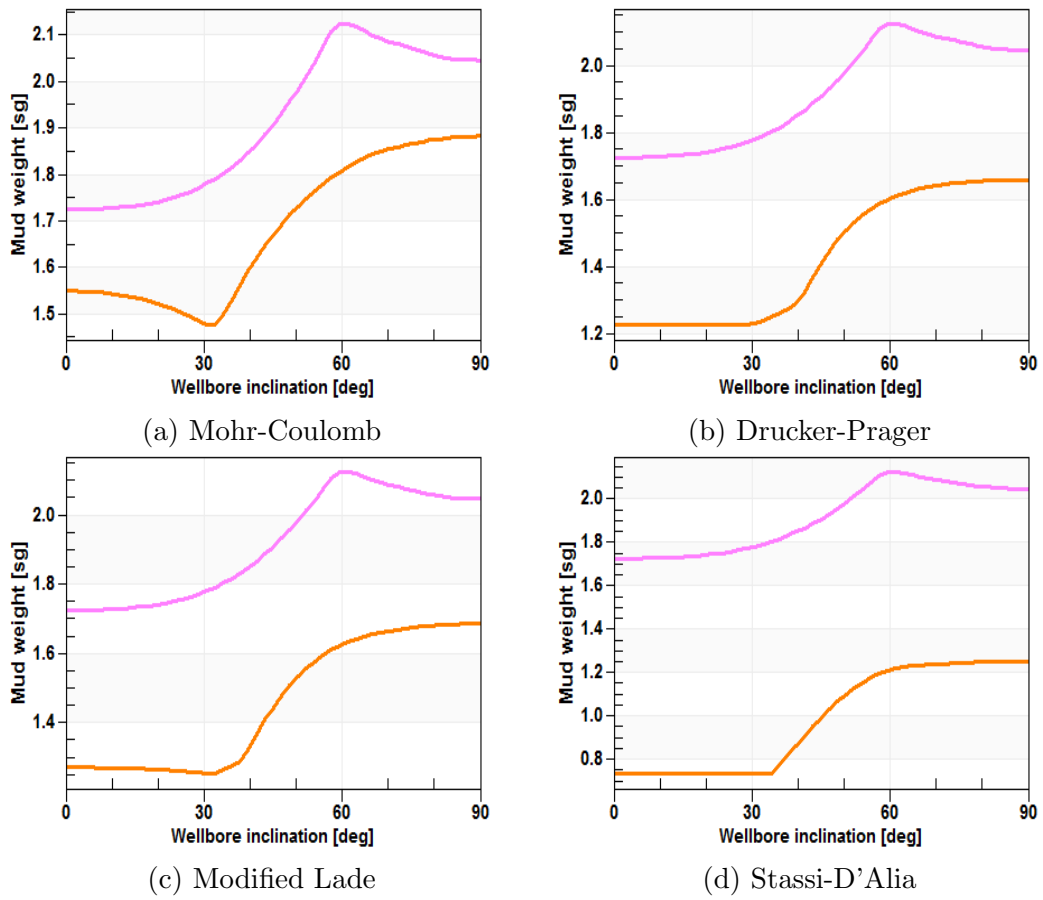


Figure 27: Comparing the four different failure criteria's inclination sensibility in case 2a regarding the mud weight window for well trajectories along the minimum horizontal in situ stress direction.

In case 2a for an inclined wellbore trajectory in the minimum horizontal in situ stress direction the mud loss pressure is estimated to be the same for all four failure criteria. This consistently coincide with the previous sensibility analyses. All four failure criteria present a possibility to drill a 90° inclined wellbore in this direction. The mud weight window for this case is widest in this direction as well for all four cases. With respect to collapse pressure exclusively, the Stassi-D'Alia is the only failure criterion that marginally prefers the direction of the maximum horizontal stress for inclinations between 35° and 50° (comparing figures 26d and 27d).

6.3.2 Azimuth sensibility case 2a

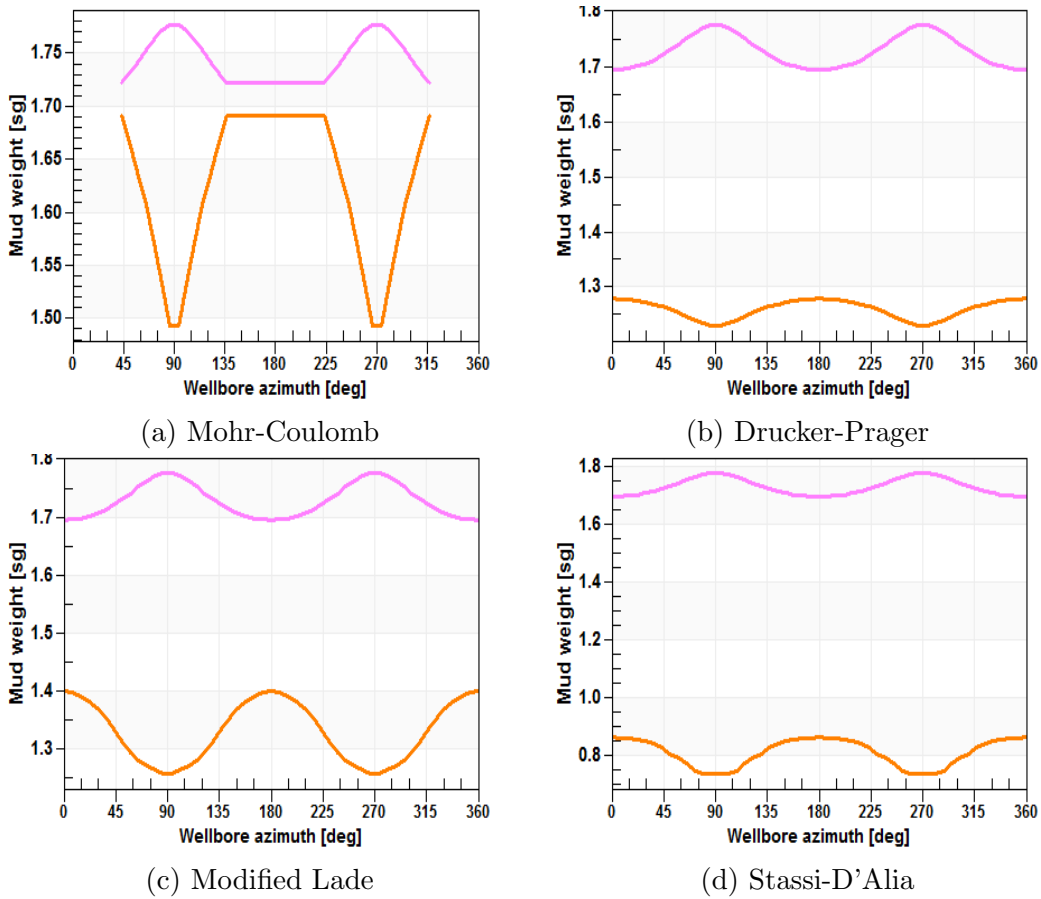


Figure 28: Comparing the four different failure criteria's azimuth sensibility in case 2a regarding the mud weight window for a 30° inclined wellbore.

For a 30° inclined wellbore the azimuth sensibility analyses in figure 28 presents what the previous two figures (27 and 26) concluded. All four failure criteria prefers the direction of the minimum horizontal stress. For the Mohr-Coulomb failure criterion the line between azimuth 135° and 225° should not exist. Comparing these results with case 1, where the azimuth sensibility regarding collapse pressure for a 30° inclined well only showed major affects for the Mohr-Coulomb failure criterion, is interesting.

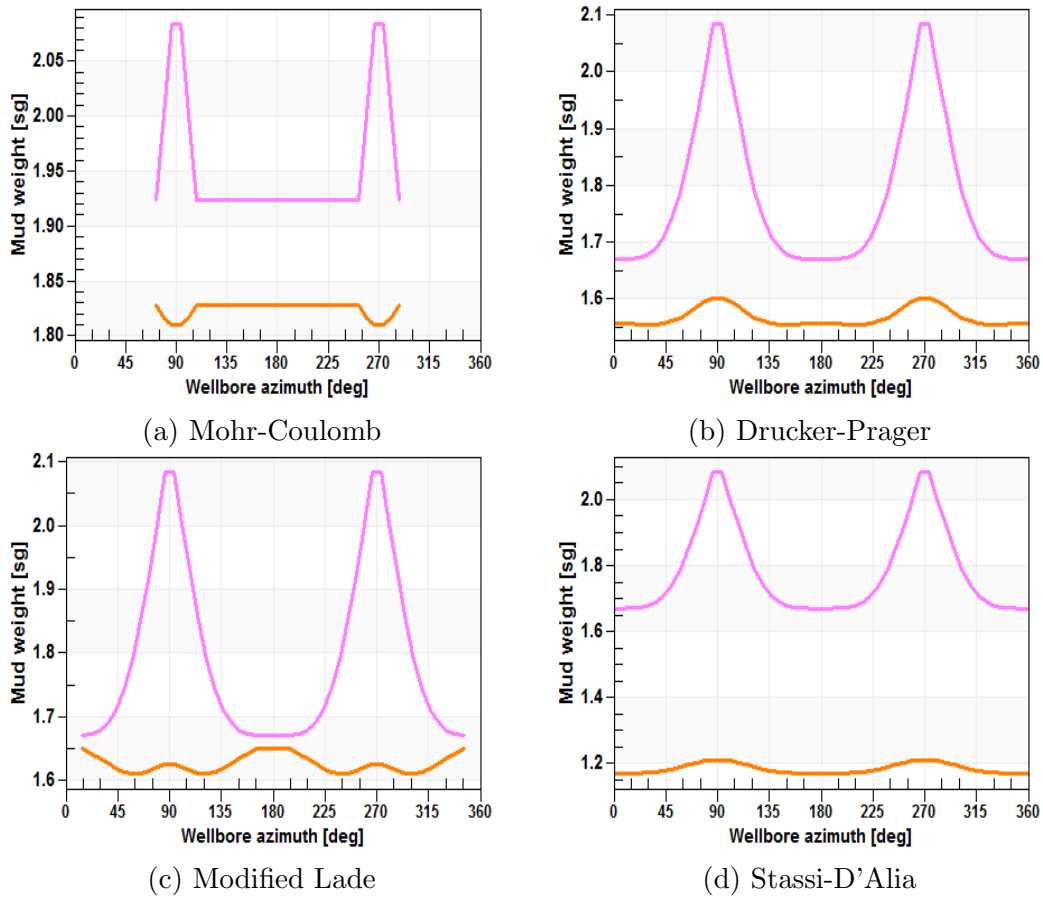


Figure 29: Comparing the four different failure criteria's azimuth sensibility in case 2a regarding the mud weight window for a 60° inclined wellbore.

Figure 26 showed that for a wellbore trajectory along the maximum horizontal in situ stress the Mohr-Coulomb and Modified Lade failure criteria predicted that it was not possible to incline the wellbore to 60° . In figure 29a the line between azimuth 112° and 248° should not exist. This is a plotting error performed by the PSI software. In a similar way one can then conclude that the line between azimuth 165° and 195° in figure 29c also is a plotting error. For a 60° inclined wellbore the Drucker-Prager and Stassi-D'Alia failure criteria presents the maximum mud weight window in the direction of the minimum horizontal in situ stress direction. This coincide with the other two failure criteria. However when only considering the collapse pressure the Drucker-Prager and Stassi-D'Alia failure criteria predicts the highest value in this very direction. This does not coincide with the other two failure criteria, and it does not coincide with the results presented in figure 28.

6.4 Matlab results case 2a

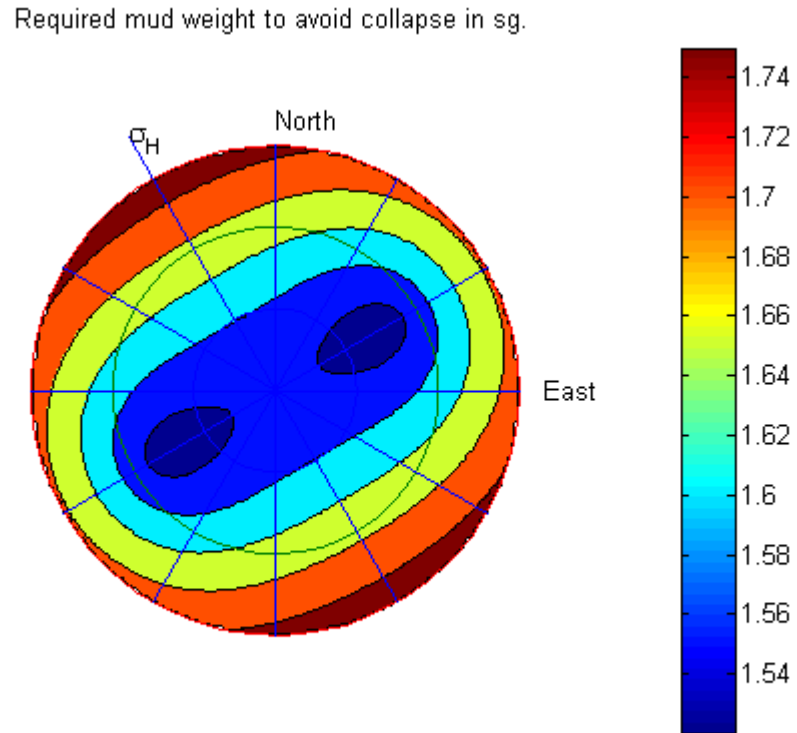


Figure 30: Minimum required mud weight to avoid collapse failure initiation in case 2a for the Mohr-Coulomb failure criterion according to the Matlab calculations.

Again the results from the Matlab calculations coincide reasonably well with the PSI simulations. Keeping in mind that the PSI requires more inputs and perform more complex calculations this is very satisfying. From the figure 30 one can easily find out the most favored deviation according to the matlab calculations performed using the Mohr-Coulomb failure criterion in case 2a.

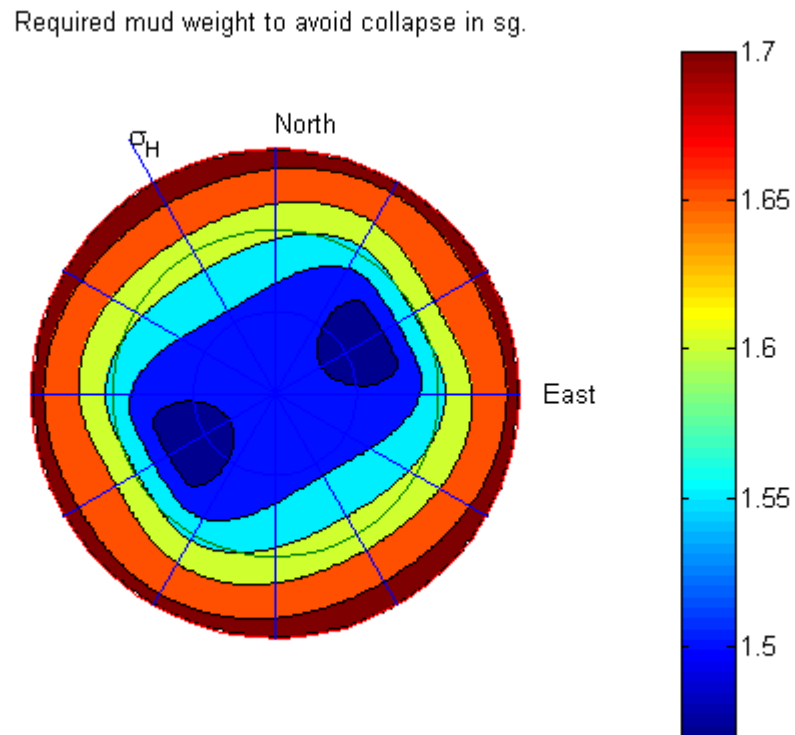


Figure 31: Minimum required mud weight to avoid collapse failure initiation in case 2a for the Mogi-Coulomb failure criterion according to the Matlab calculations.

The Mogi-Coulomb failure criterion shows the same similarity compared to the Mohr-Coulomb failure criterion as it did in case 1. Also the required mud weight to avoid collapse failure initiation is lower than the predictions provided for the Mohr-Coulomb failure criteria for any given deviation just as in case 1.

6.5 Comparing failure criteria case 2b and 2a

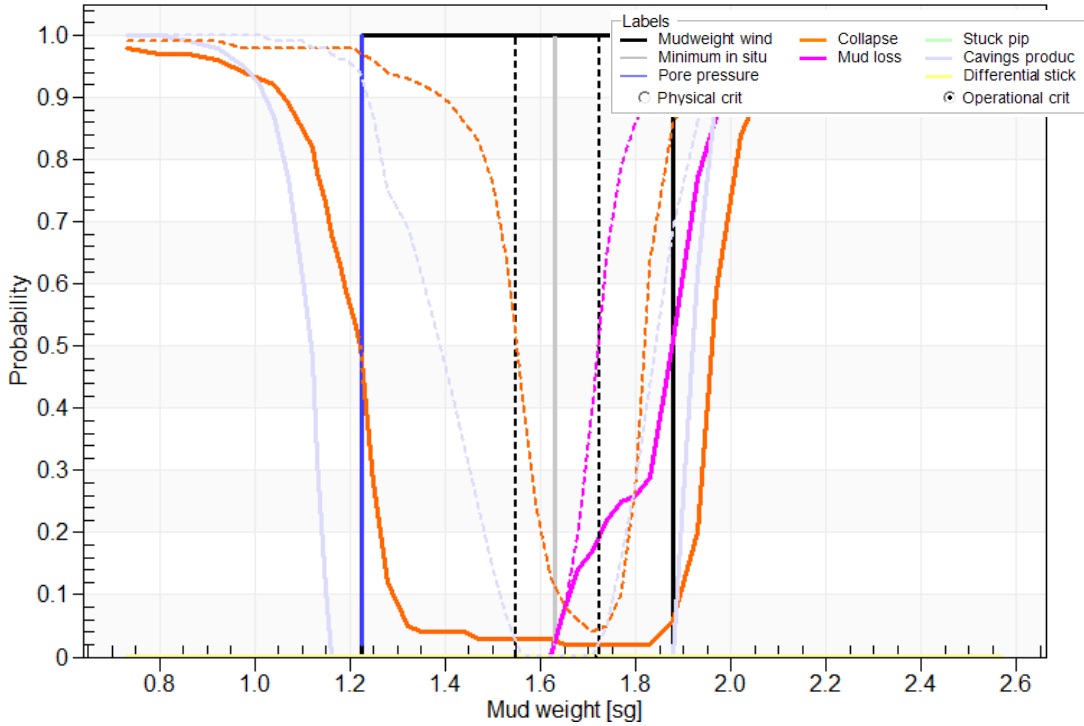


Figure 32: Mud weight window analysis for case 2b compared to case 2a (dashed) using the Mohr-Coulomb failure criterion.

Figure 32 shows a vertical well using the in situ formation stresses for case 2b (table 5) compared to case 2a using the Mohr-Coulomb failure criterion. A major increase of the mud weight window width is seen and the collapse pressure probability is 50% for a mud weight equal to the pore pressure instead of being 50% for a mud weight of 1.55 sg. The mud loss pressure is increased as well with approximately 0.15 sg.

6.5 Comparing failure criteria case 2b and 2a

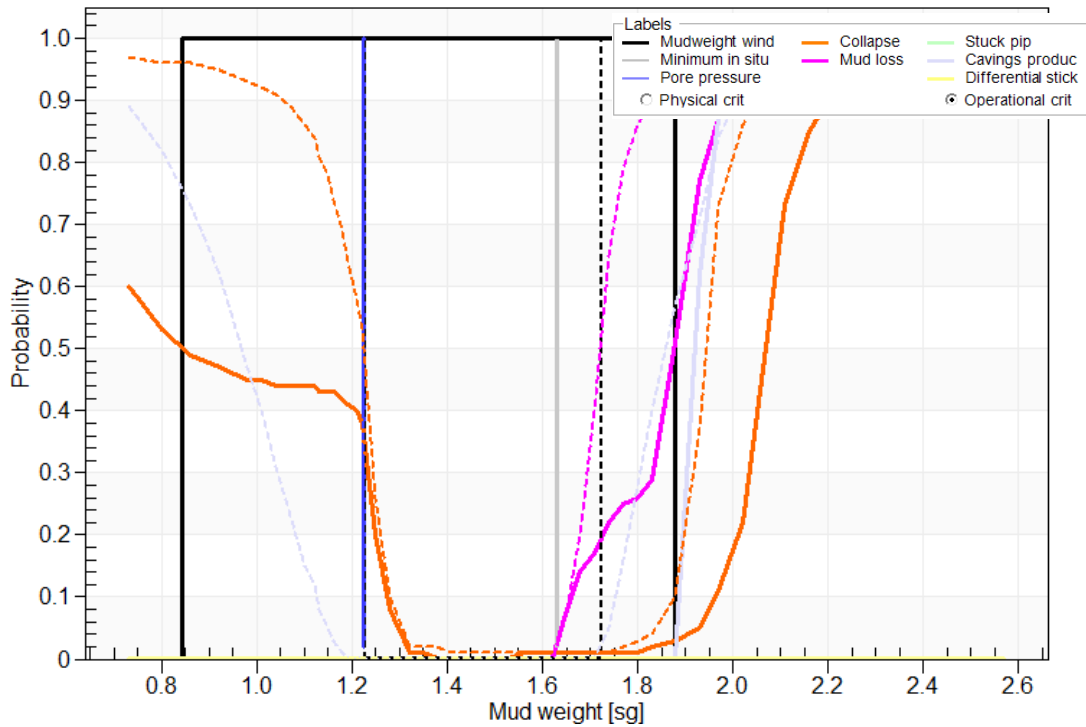


Figure 33: Mud weight window analysis for case 2b compared to case 2a (dashed) using the Drucker-Prager failure criterion.

The Drucker-Prager failure criterion also predicts an increased width of the mud weight window when comparing case 2b and 2a. In figures 32 and 33 the mud loss pressure is increased by the same amount stating that the Drucker-Prager and the Mohr-Coulomb failure criteria are consistently still putting out the same mud loss prediction regardless of the case set up. The collapse pressure is seen to increase drastically when comparing the two cases 2b and 2a using the Drucker-Prager failure criterion, but at the case 2a prediction the probability for collapse in 2c equals approximately 35% which is still relatively high.

6.5 Comparing failure criteria case 2b and 2a

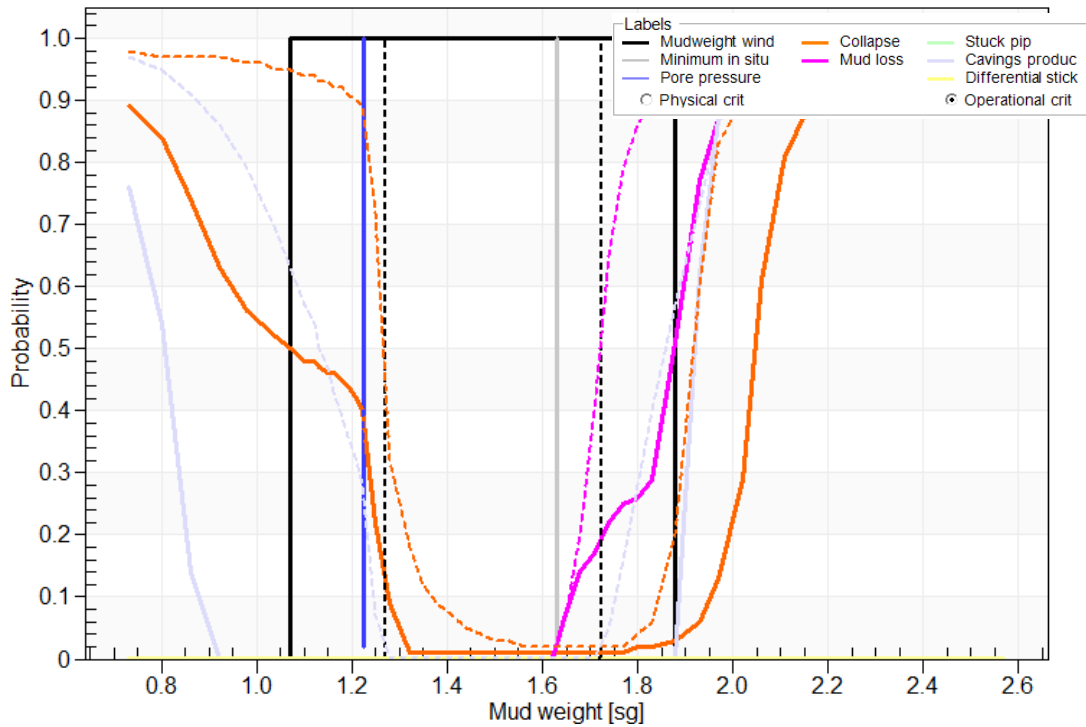


Figure 34: Mud weight window analysis for case 2b compared to case 2a (dashed) using the Modified Lade failure criterion.

The Modified Lade criterion predicts a slightly more modest increase of the mud weight window width than the Mohr-Coulomb and Drucker-Prager failure criteria when comparing case 2b and 2a. Comparing figure 34 with 33 shows that the decrease in collapse pressure, when using the Modified Lade failure criterion instead of the Drucker-Prager failure criterion, is present for all probabilities, not just for 35% probability and upwards. It can be noted that the mud loss pressure is still increased by the same amount regardless of the failure criteria used when comparing case 2b and 2a.

6.5 Comparing failure criteria case 2b and 2a

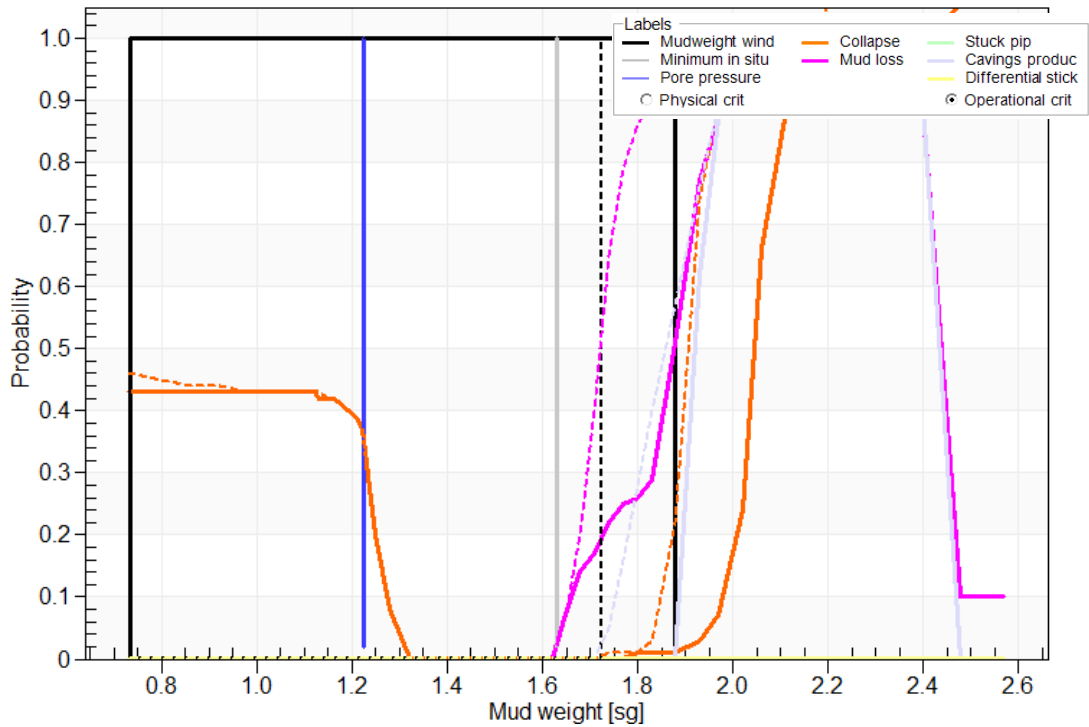


Figure 35: Mud weight window analysis for case 2b compared to case 2a (dashed) using the Stassi-D'Alia failure criterion.

The Stassi-D'Alia failure criterion also predicts the same mud loss pressure increase as the other failure criteria when comparing case 2b and 2a. Both case 2b and 2a predicts that the probability for collapse is less than 50% for a mud weight of 0.75 sg. The lower limit of the mud weight window drawn in figure 35 is therefore not correct. This explains the straight horizontal lines running from inclination 0° and 15° in figure 26d and 0° and 35° in figure 27d. These mud weight values for collapse should theoretically be lower according to Stassi-D'Alia failure criterion, but practically these values are very questionable since they do not predict higher probability for collapse below the pore pressure line. The Mohr-Coulomb failure criterion is the only failure criterion that predicts a 50% probability for collapse for an equivalent mud weight that equals the pore pressure in case 2b. The other three failure criteria predict the probability for collapse to be 30% at this point.

6.5.1 Inclination sensibility case 2b

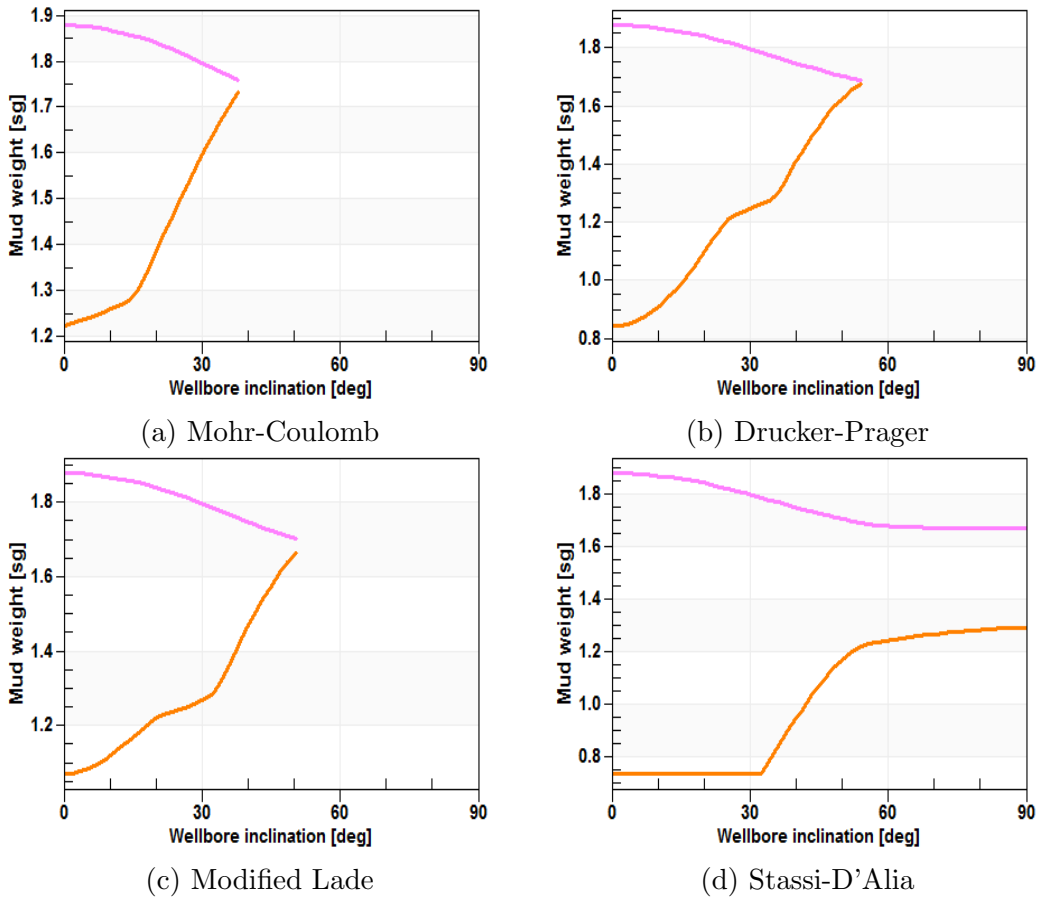


Figure 36: Comparing the four different failure criteria's inclination sensibility for the isotropic horizontal stress situation in case 2b.

In figure 36a we see a slight increase in mud weight width compared to figure 26. However the range of possible inclinations is decreased for the Drucker-Prager and Modified Lade failure criterion. The Mohr-Coulomb failure criterion predicts a slight increase in range for comparing the same figures. Case 2b assumes isotropic in situ horizontal stresses and will therefore not experience any sensibility with regards to azimuth. Case 2a predicts a possibility to drill a vertical well for all four failure criteria when doing so in the direction of the minimum horizontal in situ stress direction (fig. 27). Whereas in case 2b only the Stassi-D'Alia failure criterion predicts a possibility for an 90° inclined well.

6.6 Matlab results case 2b

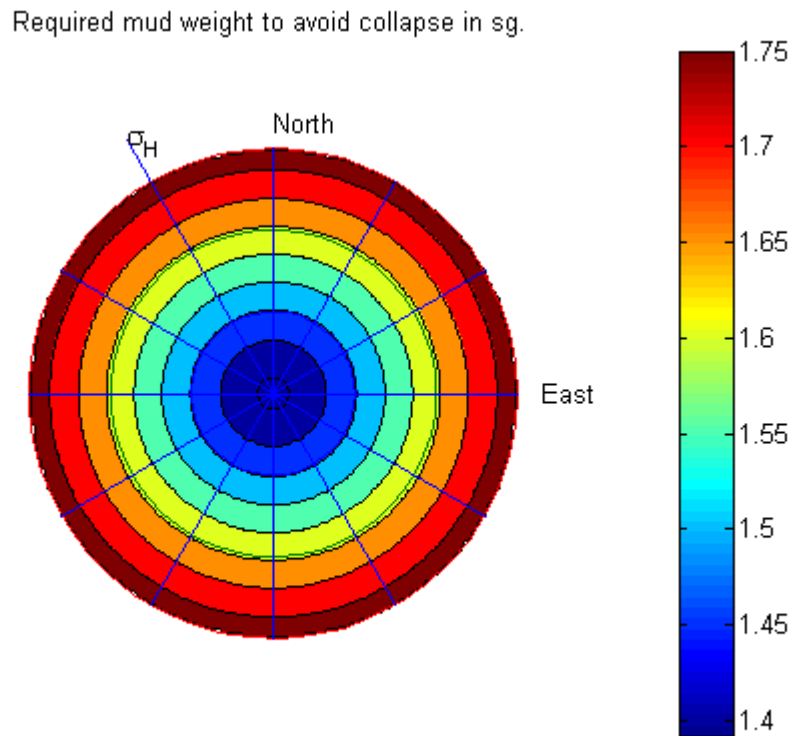


Figure 37: Minimum required mud weight to avoid collapse failure initiation in case 2b for the Mohr-Coulomb failure criterion according to the Matlab calculations.

For the isotropic horizontal stress regime in case 2b the Mohr-Coulomb failure criterion and the Mogi-Coulomb failure criterion predicts roughly the same minimum required mud weight to avoid collapse failure initiation through out all deviations. This is expected since it coincides with the theory in chapter 3.5

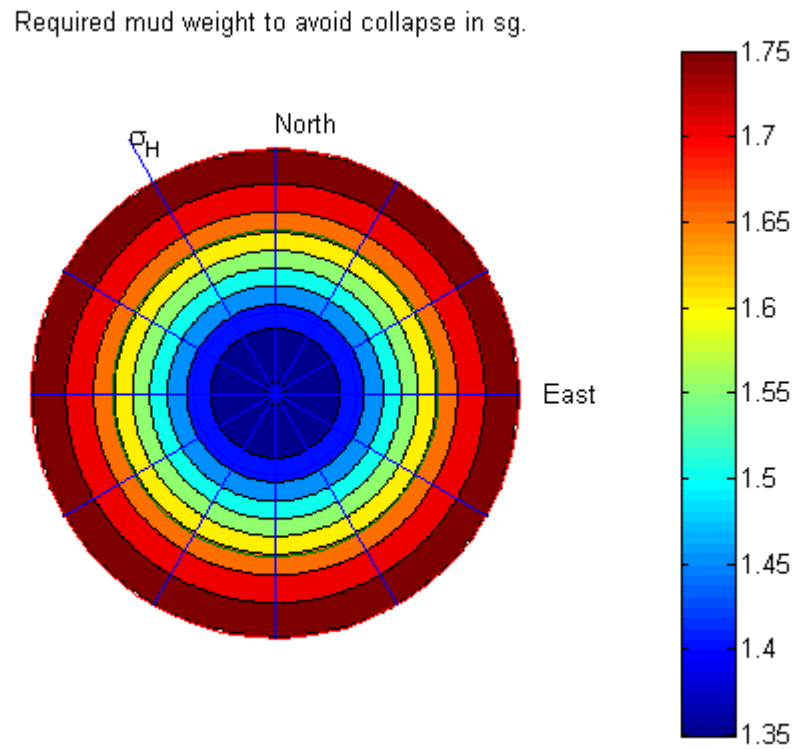


Figure 38: Minimum required mud weight to avoid collapse failure initiation in case 2b for the Mogi-Coulomb failure criterion according to the Matlab calculations.

6.7 Comparing failure criteria case 2c and 2a

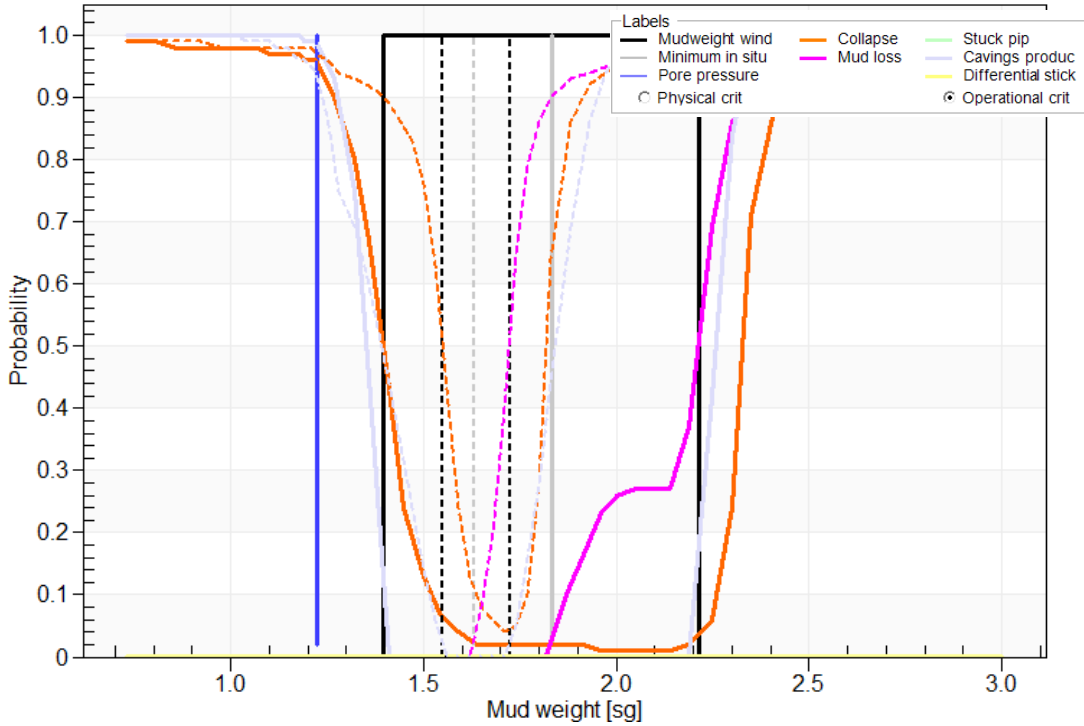


Figure 39: Mud weight window analysis for case 2c compared to case 2a (dashed) using the Mohr-Coulomb failure criterion.

The Mohr-Coulomb failure criterion predicts a lower minimum equivalent mud pressure for a vertical well in case 2c compared to 2a. The mud loss pressure is also increased. This is mainly due to the minimum in situ stress is 45 MPa and not 40 MPa. This requires a 5 MPa higher equivalent mud weight to overcome the tensile strength in the Shale.

6.7 Comparing failure criteria case 2c and 2a

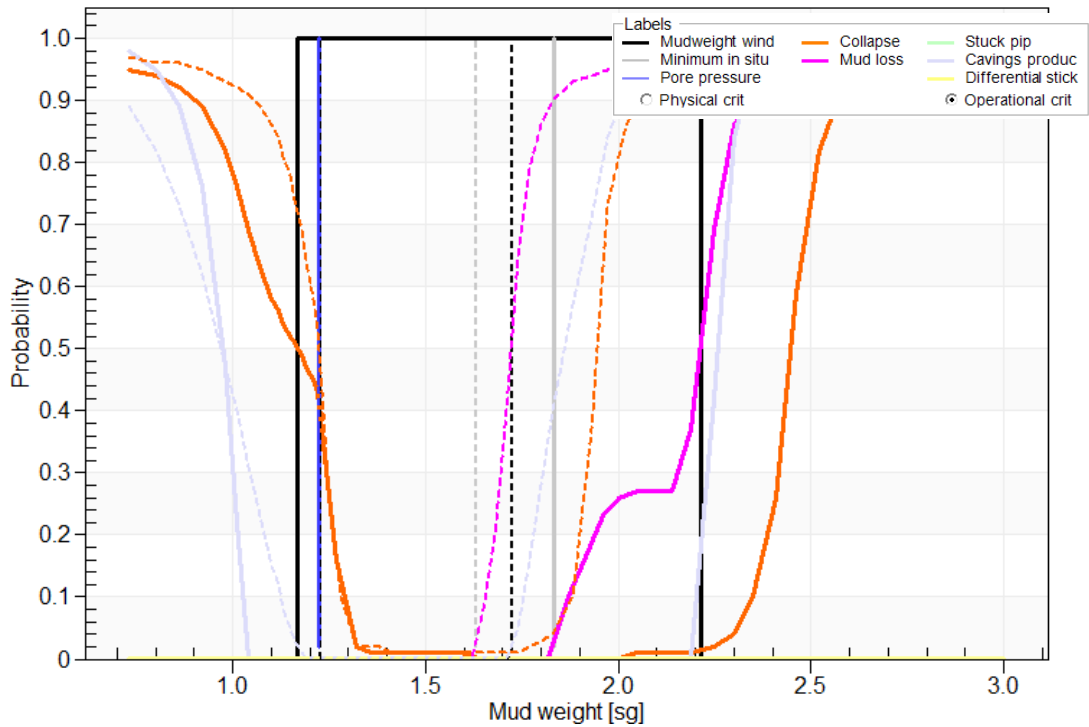


Figure 40: Mud weight window analysis for case 2c compared to case 2a (dashed) using the Drucker-Prager failure criterion.

The Drucker-Prager failure criterion increases the mud loss pressure by the same amount as the Mohr-Coulomb failure criterion in case 2c compared to case 2a. The collapse pressure prediction is almost identical when using the Drucker-Prager failure criterion in cases 2c and 2a. Prior to, and when, the probability for collapse equals 45% both cases predict the same collapse pressure.

6.7 Comparing failure criteria case 2c and 2a

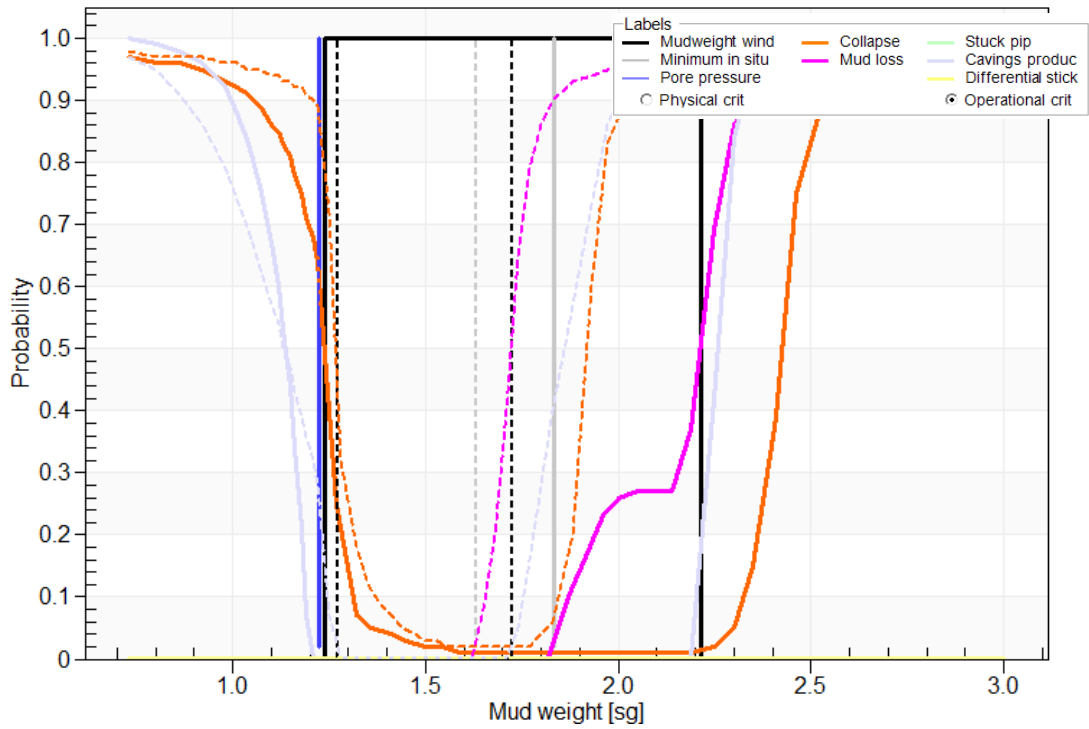


Figure 41: Mud weight window analysis for case 2c compared to case 2a (dashed) using the Modified Lade failure criterion.

The Modified Lade failure criterion predicts the same mud loss pressure increase as the previous two failure criteria for case 2c compared to case 2a. A minimal decrease in collapse pressure is also seen when comparing case 2c and 2a using this failure criterion.

6.7 Comparing failure criteria case 2c and 2a

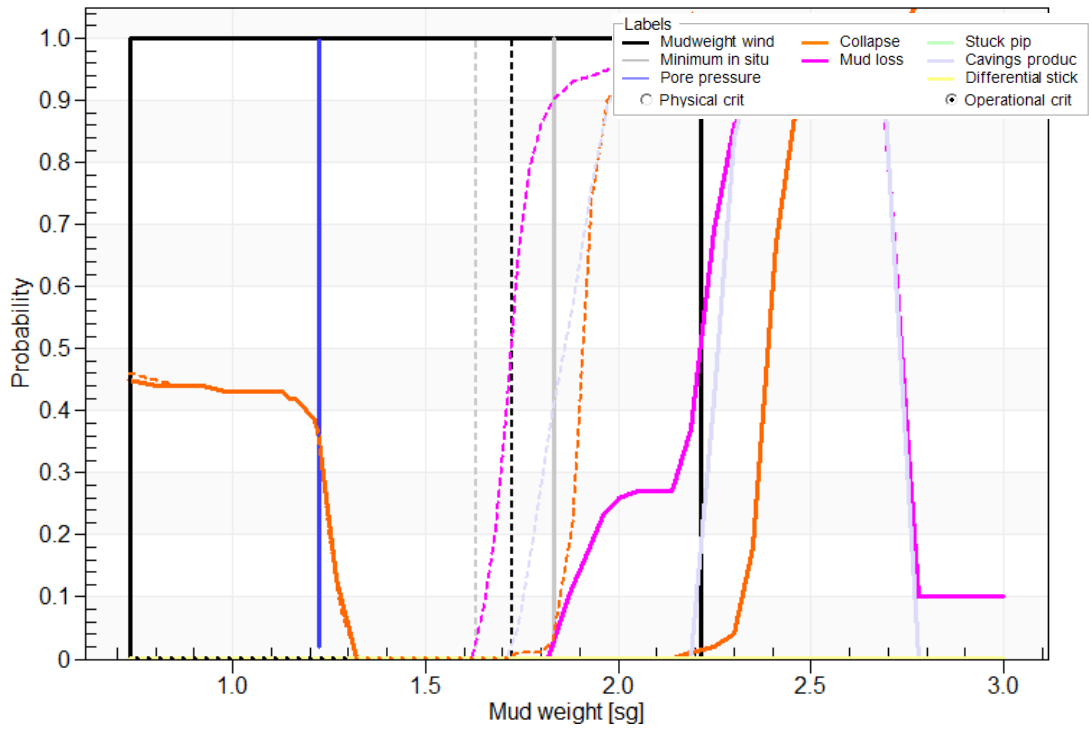


Figure 42: Mud weight window analysis for case 2c compared to case 2a (dashed) using the Stassi-D'Alia failure criterion.

The Stassi-D'Alia failure criterion follows the previously mentioned failure criteria in its prediction of the mud loss pressure. The mud loss pressure is increased when comparing case 2c and case 2a. The collapse pressure is identical for the two cases.

6.7.1 Inclination sensibility case 2c

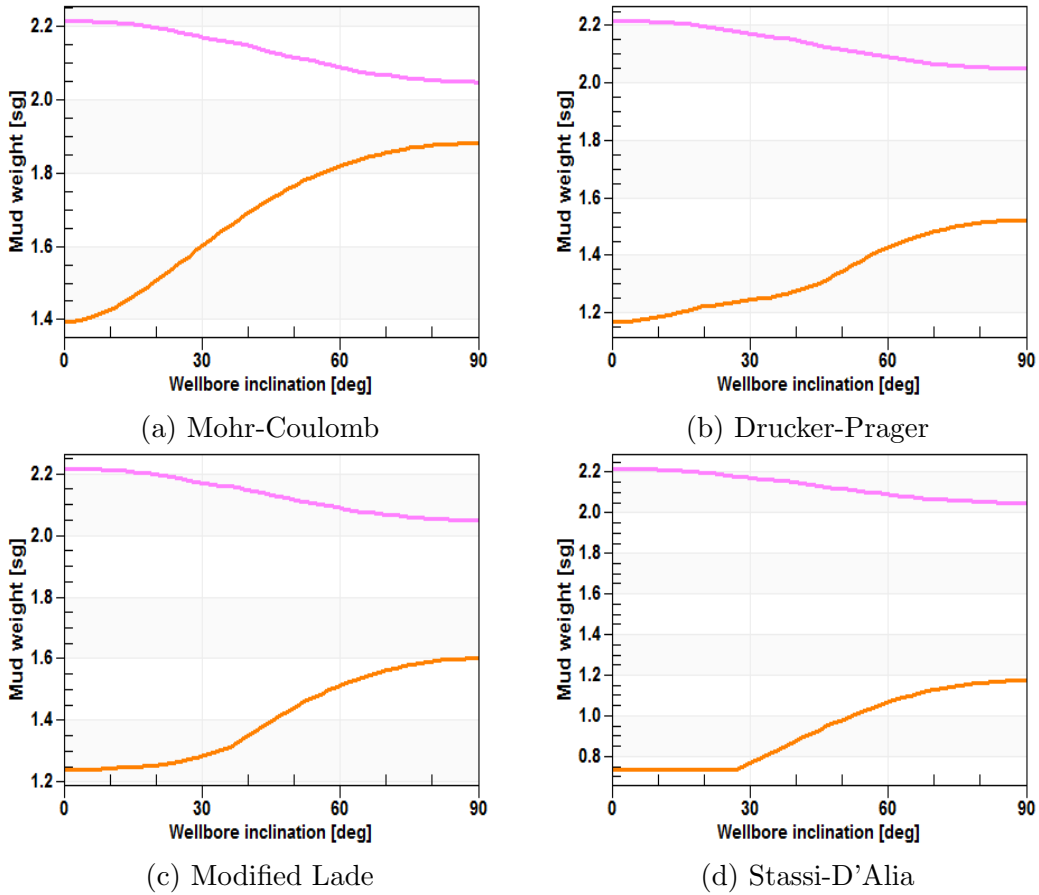


Figure 43: Comparing the four different failure criteria's inclination sensibility in case 2 regarding the mud weight window for well trajectories along the maximum horizontal in situ stress direction.

The inclination sensibility analysis for case 2c show that for this isotropic horizontal in situ stress situation all four failure criteria present a possibility to drill a horizontal well at the given true vertical depth of 2500 meters. It is interesting to note that the figures 43a and 36c reveal the exact same collapse pressure prediction at an inclination of 30° .

6.8 Matlab results case 2c

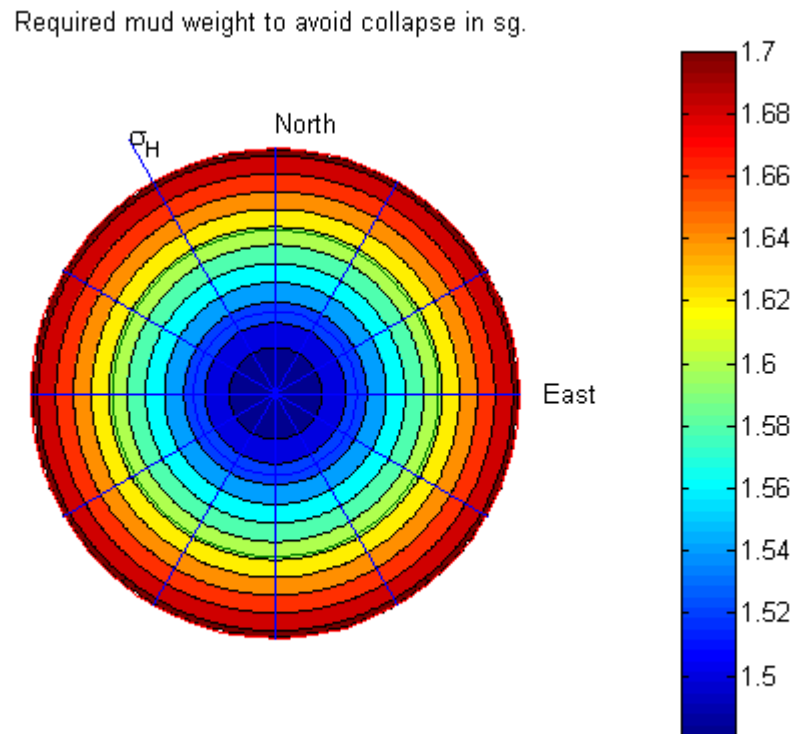


Figure 44: Minimum required mud weight to avoid collapse failure initiation in case 2c for the Mohr-Coulomb failure criteria according to the Matlab calculations.

When comparing the Mogi-Coulomb failure criterion (fig. 45) with the Mohr-Coulomb failure criterion (fig. 44) in case 2c there is a slight reduction in the required mud weigh prediction. This should not be the case according to the theory since the horizontal stress configuration is isotropic for this case. The result from case 2c should be considered as a minor uncertainty. It can maybe be solved by increasing the accuracy of the bisection method by changing the variable TolMax.

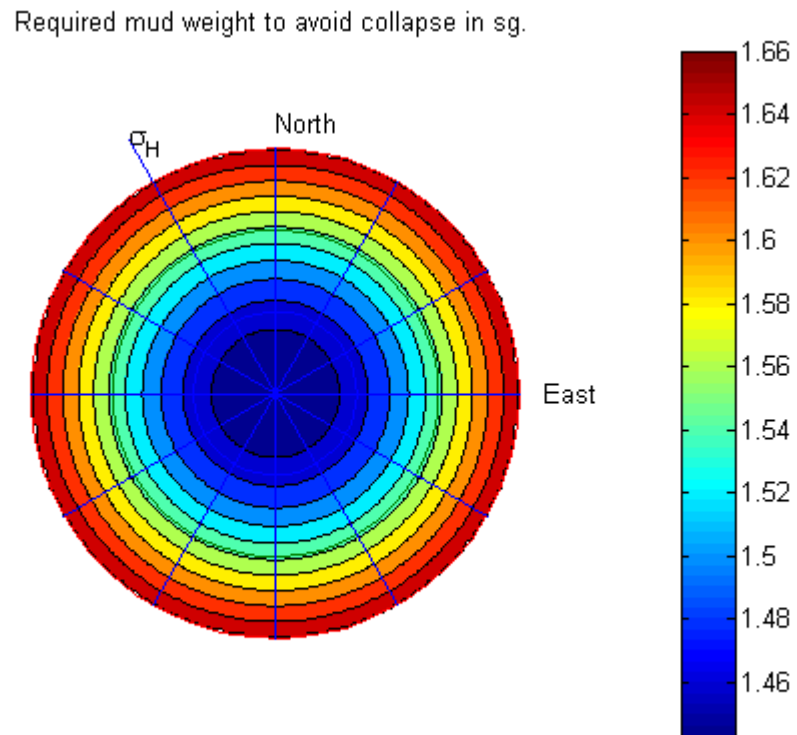


Figure 45: Minimum required mud weight to avoid collapse failure initiation in case 2c for the Mogi-Coulomb failure criteria according to the Matlab calculations.

7 Discussion

The author has focused on evaluating the different failure criteria's response to deviation of wellbores. This has been done through different assumed cases where the formation properties have been extracted from the literature. Some of the parameters required by the PSI software have not been found and therefore been kept to the default value set by PSI. Failure initiation at the borehole wall has been evaluated in this thesis in order to keep some consistency between the matlab calculations and the PSI simulations. From an operational viewpoint failure initiation at the borehole wall leading to breakouts may not necessarily jeopardies the wellbore or further drilling. However when breakouts do occur, the cylinder shaped geometry of the wellbore will ultimately change. This will question the validity of the Kirsch solution for stresses at the wellbore wall.

Factors like plasticity, time dependent effects, thermal effects, poroelasticity have automatically been considered in the PSI simulations through default values and approximate assumptions made by the author. The matlab calculations does however treat the formation as an isotropic elastic material where failure is assumed to be perfectly brittle. The only formation properties that are considered by the Matlab program are C_0 , φ and ν_{fr} . This explains the difference between the two different output methods. The validity of the case assumptions have somewhat been of lesser concern and the formation conditions used has mainly been chosen in order to find clear differences between the different failure criteria's sensibility to inclination and azimuth.

The results showed an extreme consistency for mud loss prediction. Within every case all four failure criteria predicted approximately the same mud loss pressure. This is believed to be due to the assumed low tensional strength for the formation. Therefore tensional failure will always occur prior to fracturing caused by shear failure explained in table 1. Tensional failure for a vertical well is then almost completely governed by the lowest principal stress and the relationship between the horizontal stresses and the choice of failure

criterion for evaluating mud loss becomes less important. The isotropic horizontal in situ stresses in case 2b and case 2c showed an increase of the mud weight window compared to case 2a. That can be explained by the isotropic horizontal stresses which create an even distributed total stress around the whole wellbore.

Regarding the collapse pressure the Stassi-D'Alia failure criterion consistently predicts the lowest results. From the vertical well analyzes one can note that the Stassi-D'Alia failure criteria always predict a 35% probability for collapse at the pore pressure line. Once passed that pressure the probability increase rate declines drastically and so the collapse pressure that goes in to the inclination and azimuth sensibility analyzes are vastly under-predicted. The author is not certain on why this may be but suspect that it could be some software effect in PSI due to fact that the wellbore wall failure initiation is only considered. The Drucker-Prager failure criterion predictions imitate this behavior to some extent as well.

From the sensibility analyzes in case 1 one can note that the failure criteria predict different optimal deviations with respect to collapse. The Modified Lade failure criterion seems rather neutral in this case whereas the Mohr-Coulomb and the Mogi-Coulomb failure criteria clearly state that a wellbore trajectory along the minimum horizontal in situ stress direction is beneficial. The two other failure criteria predict the the opposite and suggest a wellbore trajectory along the maximum horizontal in situ stress direction. This conflict can also be seen in figure 29 and has therefore encourage the author to conclude that different failure criteria predict different optimal deviations of the wellbore with respect to collapse. The Mohr-Coulomb failure criterion collapse pressure predictions obtained from the matlab program are consistent with the sensibility analyzes performed in PSI. A slight increase of the value is seen when comparing the two methods in each case. This is mainly due to how and when each method define the probability for collapse. The Mogi-Coulomb failure criterion prediction for collapse coincide with the literature stating that compared to the Mohr-Coulomb failure criterion the Mogi-Coulomb failure criterion should predict a lower collapse pressure.

8 Recommendations

The author would like to encourage future development and improvements of the Matlab program provided in appendix B. The next step would be to include more failure criteria into the code and also account for anisotropic failure criteria. For future development of the PSI software the author recommends that some emphasis is devoted to the output presentation. This may improve the user experience for users which are not that experienced in the field of formation mechanics. In the petroleum industry today the boarders between different areas of expertise are vanishing and softwares need to reach out to teams containing people with a wide range of backgrounds.

9 Conclusion

Four different failure criteria have been compared and tested in four different assumed cases. The failure criteria's sensibility to different deviations have been analyzed. Additionally a Matlab program has been written in order to enhance the authors knowledge in mud weight prediction calculations and to compare the Mogi-Coulomb failure criterion with the Mohr-Coulomb failure criterion. From the results and work of compiling this thesis the following conclusions have been made:

- Different failure criteria predicts different optimal deviation for a given case. Choosing the right criterion is critical to obtain the best practical outcome.
- Calculations performed in the Matlab program coincide with the theory and the PSI simulations and can therefore be regarded as a successful project. Also it is a fast and convenient way to find the most beneficial deviation for a wellbore according to the chosen failure criterion.
- An isotropic horizontal in situ stress situation is beneficial for vertical wells.
- The Mogi-Coulomb and Mohr-Coulomb failure criteria predicts the same optimal deviation concerning the collapse pressure.
- The Drucker-Prager and Stassi-D'Alia failure criteria behaves similarly with respect to deviation sensibility.
- The Mohr-Coulomb criterion conservatively predicts the highest required minimum mud weight to avoid collapse for all cases.
- The choice of failure criteria is not critical when predicting mud loss.

References

- [Al-Ajmi and Zimmerman, 2005] Al-Ajmi, A. M. and Zimmerman, R. W. (2005). Relation between the mogi and the coulomb failure criteria. *International Journal of Rock Mechanics and Mining Sciences*, 42(3):431–439.
- [Al-Ajmi and Zimmerman, 2006] Al-Ajmi, A. M. and Zimmerman, R. W. (2006). Stability analysis of vertical boreholes using the mogi–coulomb failure criterion. *International Journal of Rock Mechanics and Mining Sciences*, 43(8):1200–1211.
- [Ewy et al., 1999] Ewy, R. et al. (1999). Wellbore-stability predictions by use of a modified lade criterion. *SPE Drilling & Completion*, 14(02):85–91.
- [Fjær et al., 2008] Fjær, E., Holt, R. M., Horsrud, P., Raaen, A. M., and Risnes, R. (2008). *Petroleum Related Rock Mechanics*. Elsevier, 2nd edition.
- [Gueguen and Bouteica, 1999] Gueguen, Y. and Bouteica, M. (1999). Mechanical properties of rocks: pore pressure and scale effects. *Oil & Gas Science and Technology*, 54(6):703–714.
- [Horsrud et al., 1998] Horsrud, P., Sønstebo, E., and Bøe, R. (1998). Mechanical and petrophysical properties of north sea shales. *International Journal of Rock Mechanics and Mining Sciences*, 35(8):1009–1020.
- [Jaeger et al., 2007] Jaeger, J. C., Cook, N. G., and Zimmerman, R. (2007). *Fundamentals of rock mechanics*. Blackwell, 4th edition.
- [Kvevik et al., 2013] Kvevik, G., Manalac, E., Stevenson, N., Persson, C., Dorr, J., et al. (2013). Reducing brownfield development costs via improved drilling practice and enhanced understanding of wellbore instability in weak formations. In *SPE Annual Technical Conference and Exhibition*. Society of Petroleum Engineers.

- [Martin et al., 1999] Martin, C., Kaiser, P., and McCreath, D. (1999). Hoek-brown parameters for predicting the depth of brittle failure around tunnels. *Canadian Geotechnical Journal*, 36(1):136–151.
- [Mogi, 1971] Mogi, K. (1971). Fracture and flow of rocks under high triaxial compression. *Journal of Geophysical Research*, 76(5):1255–1269.
- [Rahimi et al., 2014] Rahimi, R., Nygaard, R., et al. (2014). What difference does selection of failure criteria make in wellbore stability analysis? In *48th US Rock Mechanics/Geomechanics Symposium*. American Rock Mechanics Association.
- [Stassi-D’Alia, 1967] Stassi-D’Alia, F. (1967). Flow and fracture of materials according to a new limiting condition of yielding. *Meccanica*, 2(3):178–195.
- [Zhang et al., 2010] Zhang, L., Cao, P., and Radha, K. (2010). Evaluation of rock strength criteria for wellbore stability analysis. *International Journal of Rock Mechanics and Mining Sciences*, 47(8):1304–1316.

Appendix A Failure criteria comparison

A.1 Case 1

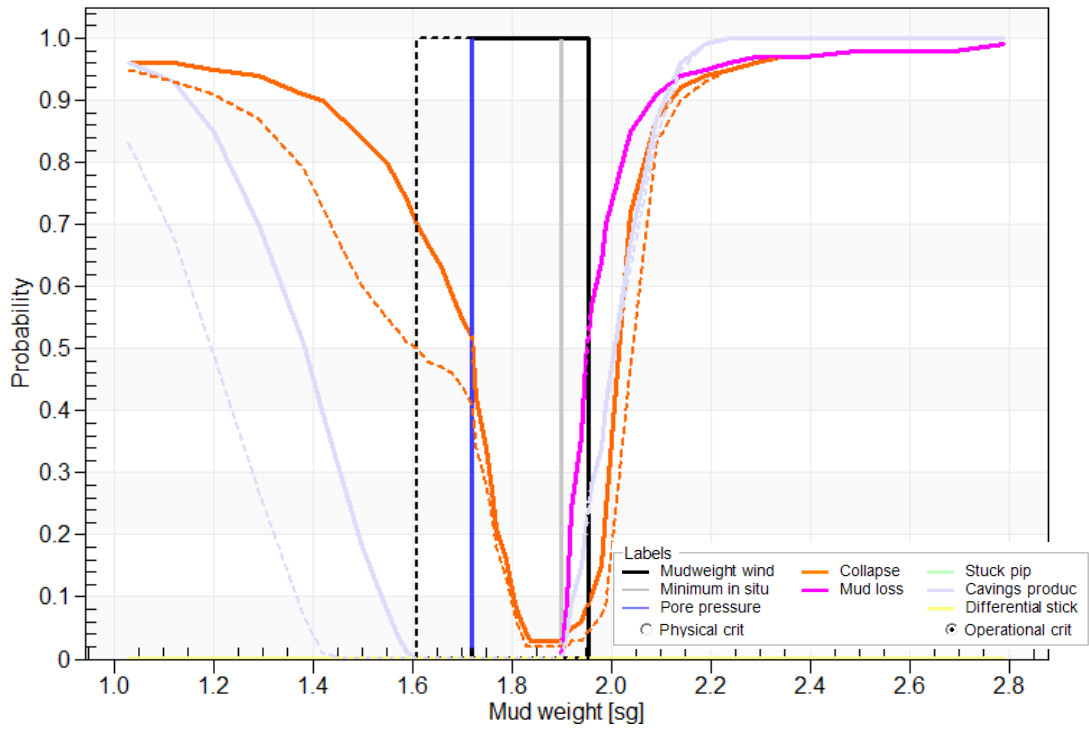


Figure A1: Mud-weight window analysis for case 1 comparing the Modified Lade failure criterion with the Drucker-Prager failure criterion (dashed).

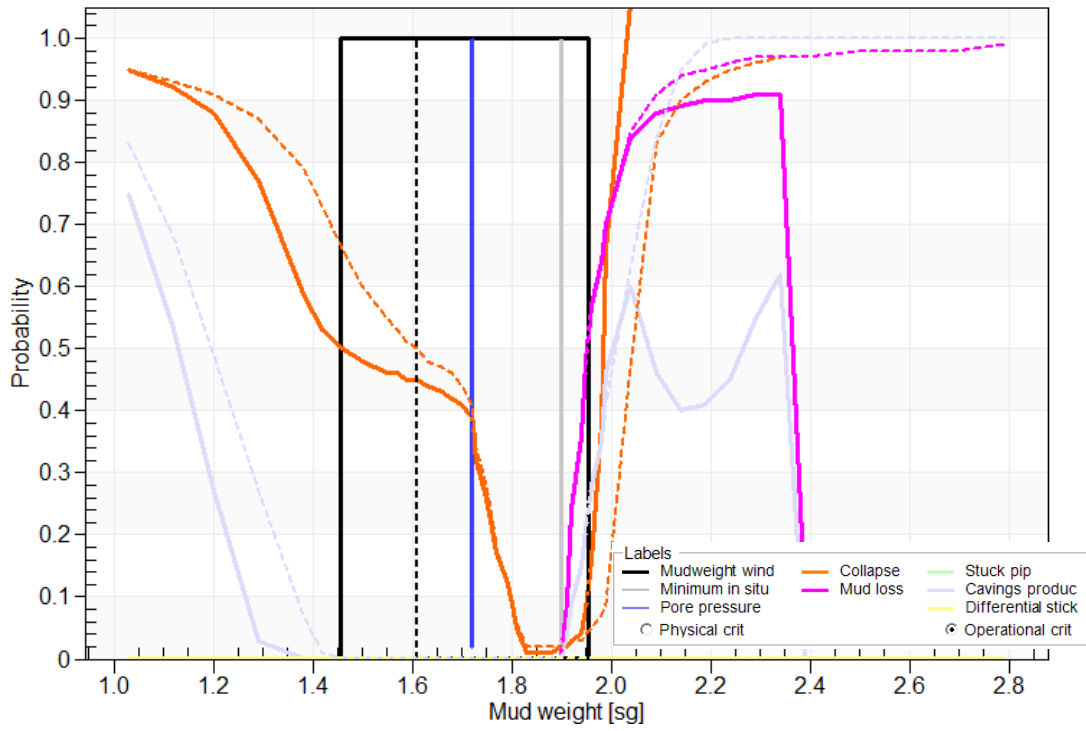


Figure A2: Mud-weight window analysis for case 1 comparing the simplified Stassi D'alia failure criterion with the Drucker-Prager failure criterion (dashed).

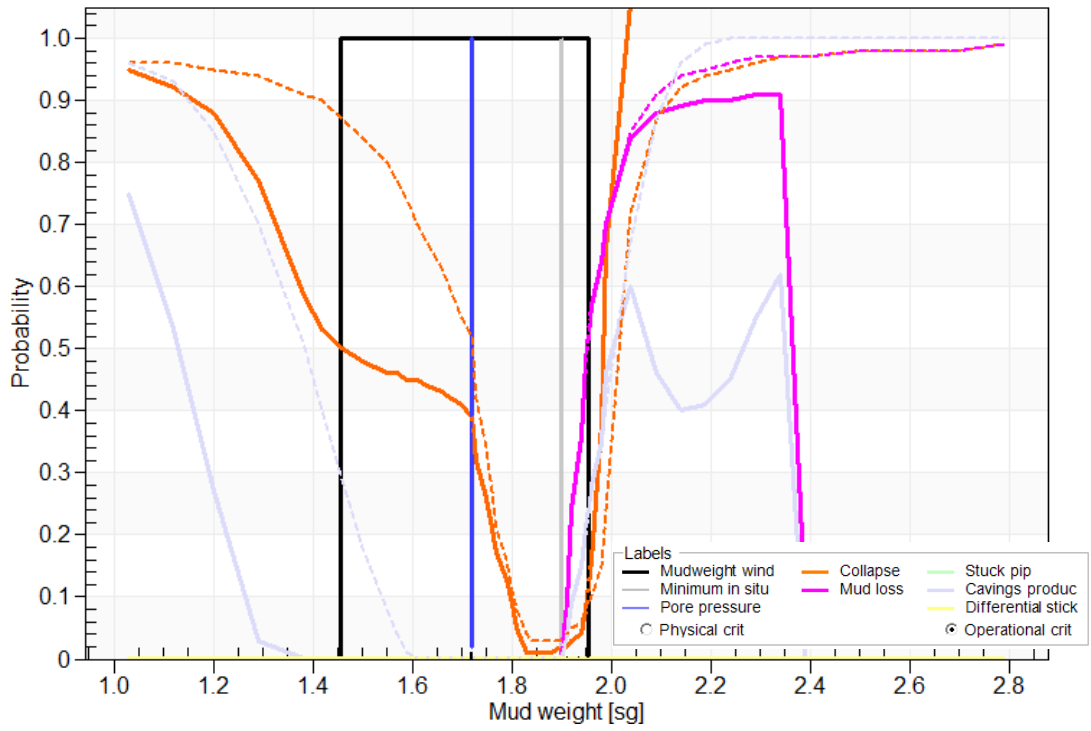


Figure A3: Mud-weight window analysis for case 1 comparing the simplified Stassi D'alia failure criterion with the Modified Lade failure criterion (dashed).

Appendix B Matlab scripts

B.1 Transformation formulas

B.1.1 Tensor set up

```

%Principal stresses to geographical stress tensor!
% ----- %

%Organizing the principal stresses into a stress tensor.
% ----- %

function [SprT]=stress2tensor(SH,Sh,Sv)

sp = [ Sh; SH ; Sv];
SprT = diag(sp);
end

```

B.1.2 In situ stress tensor to geographical tensor

```

%Principal stresses to geographical stress tensor!
% ----- %

%This function takes in the principal stresses (Sv, SH and Sh) and the
%angles (alpha, beta and gamma needed to rotate the principal stress tensor
%to a geographic stress tensor.

% ----- %

function [Sg] = GeoStress(S,alpha,beta,gamma)
% ----- %

%Set up the transformation matrix (Rg) that transforms the
%principal stress tensor (S) to a geographic stress tensor (Sg):

Rg = [cosd(alpha)*cosd(beta) sind(alpha)*cosd(beta) -sind(beta);

```

```

cosd(alpha)*sind(beta)*sind(gamma)-sind(alpha)*cosd(gamma) ...
cosd(alpha)*cosd(gamma)+sind(alpha)*sind(beta)*sind(gamma) ...
cosd(beta)*sind(gamma);
sind(alpha)*sind(gamma)+cosd(alpha)*sind(beta)*cosd(gamma) ...
sind(alpha)*sind(beta)*cosd(gamma)-cosd(alpha)*sind(gamma) ...
cosd(beta)*cosd(gamma)];
% ----- %

%Calculate the geographical stress tensors Sg:

Sg = Rg'*(S*Rg);
% ----- %

end

```

B.1.3 Geographical stress tensor to wellbore tensor

```

%Geografical stresses to Wellbore stress tensor!
% ----- %

%This function takes in the geographical stress tensor (S) and transform it
%to a wellbore stress tensor by taking in the Azimuth (Az) of the wellbore
%toe to north, and the inclination (Inc) of the the wellbore.

% ----- %

function [Sb] = Geo2WellStress(S,alpha,beta,gamma,Az,Inc)
% ----- %

%Set up the borehole transformation matrix:

Rb = [ cosd(Az)*cosd(Inc)  sind(Az)*cosd(Inc)  -sind(Inc)
       -sind(Az)           cosd(Az)           0.0
       cosd(Az)*sind(Inc)  sind(Az)*sind(Inc)  cosd(Inc)   ];
% ----- %

%Call in Geographical stress tensor:

```

B.2 Stresses around the wellbore

```
Sg = GeoStress(S, alpha, beta, gamma);  
% ----- %  
  
%Calculate the borehole stress tensor Sb:  
  
Sb = Rb * Sg * Rb';  
% ----- %  
  
end
```

B.2 Stresses around the wellbore

B.2.1 General elastic solution

```
%General elastic solution!  
% ----- %  
  
%This function calculates the elastic stresses around wells. For Rw=r the  
%stresses at the wellbore wall are found.  
  
% ----- %  
  
function [Sr, St, Sz, Ttz, Trt, Trz] = WellWallStress(S, fish, theta, Dp, Rw, r)  
% ----- %  
  
Sr = 0.5*(S(1,1)+S(2,2))*(1-(Rw^2/r^2)) ...  
    +0.5*(S(1,1)-S(2,2))*(1+(3*Rw^4/r^4)-(4*Rw^2/r^2))*cosd(2*theta) ...  
    +S(1,2)*(1+(3*Rw^4/r^4)-(4*Rw^2/r^2))*sind(2*theta)+Dp*(Rw^2/r^2);  
  
St = 0.5*(S(1,1)+S(2,2))*(1+(Rw^2/r^2)) ...  
    -0.5*(S(1,1)-S(2,2))*(1+(3*Rw^4/r^4))*cosd(2*theta) ...  
    -S(1,2)*(1+(3*Rw^4/r^4))*sind(2*theta)-Dp*(Rw^2/r^2);  
  
Sz = S(3,3)-fish*(2*(S(1,1)-S(2,2))*(Rw^2/r^2)*cosd(2*theta) ...  
    +4*S(1,2)*(Rw^2/r^2)*sind(2*theta));  
  
Trt = 0.5*(S(2,2)-S(1,1))*(1-(3*Rw^4/r^4)+(2*Rw^2/r^2))*sind(2*theta) ...  
    +S(1,2)*(1-(3*Rw^4/r^4)+(2*Rw^2/r^2))*cosd(2*theta);
```

```
Ttz = (S(2,3)*cosd(theta)-S(1,3)*sind(theta))*(1+(Rw^2/r^2));  
Trz = (S(2,3)*cosd(theta)+S(1,3)*sind(theta))*(1-(Rw^2/r^2));  
  
end
```

B.2.2 Principal stresses

```
%Finding the principal stresses at a surface perpendicular to the wellbore  
%axis.  
% ----- %  
  
%This function calculates the principal stresses at a surface perpendicular  
%to the wellbore axis. If Rw=r the principal stresses at the wellbore wall  
%are found.  
  
% ----- %  
  
function [Stmax,Stmin] = PrinsWellbore(S, fish, theta, Dp, Rw, r)  
% ----- %  
  
[St,Sz,Ttz] = WellWallStress(S, fish, theta, Dp, Rw, r);  
  
Stmax = (0.5)*(Sz+St+sqrt((Sz-St).^2+4*Ttz.^2));  
  
Stmin = (0.5)*(Sz+St-sqrt((Sz-St).^2+4*Ttz.^2));  
  
end
```

B.3 Failure criteria functions

B.3.1 Mohr-Coulomb Newton's method

```

%Mohr-Coulomb failure criteria function using Newton's method!
% ----- %

%This function calculates the required equivalent mud weight to avoid
%collapse failure initiation using the Mohr-Coulomb failure criteria in
%combination with the Newton-Rapson iteration method

% ----- %

function [Pm_min, M] = required_Pm(S,Pp, fish,muint, aaa,bbb,ggg,Az...
    ,Inc,C_0,Depth)

Fr = 45+(muint/2);
D = 2*tand(Fr)^2;
S = Geo2WellStress(S,aaa,bbb,ggg,Az,Inc);

thetatheta = linspace(0,360,360);

n = length(thetatheta);
M=zeros(1,n);
for i = 1:n
    theta=thetatheta(i);
    Sz = S(3,3)-fish*(2*(S(1,1)-S(2,2))*cosd(2*theta)...
        +4*S(1,2)*sind(2*theta))-Pp;

    Ttz =2*(S(2,3)*cosd(theta)-S(1,3)*sind(theta));

    A = S(1,1)+S(2,2)-2*(S(1,1)-S(2,2))*cosd(2*theta)...
        -4*S(1,2)*sind(2*theta)-Pp+Sz;

    B = S(1,1)+S(2,2)-2*(S(1,1)-S(2,2))*cosd(2*theta)...
        -4*S(1,2)*sind(2*theta)-Pp-Sz;

    C = 4*Ttz^2;

```

```

% ----- %
Pwmin=36;
nmax=25;
eps=1;
nn=0;

while eps>=1e-2&&nn<=nmax
    yy=Pwmin-(A-2*C_0+D*Pp+sqrt((B-Pwmin)^2+C)-Pwmin*(1+D))...
        /(((Pwmin-B)/(sqrt((B-Pwmin)^2+C)))-D-1);
    eps=abs(yy-Pwmin);
    Pwmin=yy;nn=nn+1;
end
% ----- %

M(1,i)=Pwmin;
end
Pm_min = max(M)/(0.00981*Depth);
end

```

B.3.2 Mohr-Coulomb bisection method

```

%Mohr-Coulomb failure criteria set up for Bisection method!
% ----- %
function [Pm_min] = R_pmBis(S,Pp, fish,muint,aaa,bbb,ggg,Az, Inc,C_0,Depth)

Fr = 45+(muint/2);
S = Geo2WellStress(S,aaa,bbb,ggg,Az, Inc);

thetatheta = linspace(0,360,360);

n = length(thetatheta);
M=zeros(1,n);
for i = 1:n
    theta=thetatheta(i);
    Sz = S(3,3)-fish*(2*(S(1,1)-S(2,2))*cosd(2*theta)...
        +4*S(1,2)*sind(2*theta))-Pp;

```



```

Ttz =2*(S(2,3)*cosd(theta)-S(1,3)*sind(theta));

A = S(1,1)+S(2,2)-2*(S(1,1)-S(2,2))*cosd(2*theta)...
    -4*S(1,2)*sind(2*theta)-Pp+Sz;

B = S(1,1)+S(2,2)-2*(S(1,1)-S(2,2))*cosd(2*theta)...
    -4*S(1,2)*sind(2*theta)-Pp-Sz;

C = 4*Ttz^2;

D = 2*tand(Fr)^2;

fun = @(x) A-2*C_0+D*Pp+sqrt((B-x)^2+C)-x*(1+D);
a = 20;
b = 40;
TolMax = 0.01;
c = Bisection(fun,a,b,TolMax);

M(1,i) = c;
end

Pm_min = max(M)/(0.00981*Depth);

end

```

B.3.3 Mogi-Coulomb bisection method

```

%Mogi-Coulomb failure criteria function!
% ----- %

%This function calculates the required equivalent mud weight to avoid
%collapse failure initiation using the Mogi-Coulomb failure criteria in
%combination with the Bisection iteration method.

% ----- %

function [Pm_min] = MogiCol(S,Pp, fish,muint,aaa,bbb,ccc,Az,Inc,C_0,Depth)

```

B.3 Failure criteria functions

```

Fr = 45+(mu*int/2);
S = Geo2WellStress(S,aaa,bbb,ccc,Az,Inc);

thetatheta = linspace(0,360,360);

n = length(thetatheta);
M=zeros(1,n);
for i = 1:n
    theta=thetatheta(i);
    Sz = S(3,3)-fish*(2*(S(1,1)-S(2,2))*cosd(2*theta)...
        +4*S(1,2)*sind(2*theta))-Pp;

    Ttz =2*(S(2,3)*cosd(theta)-S(1,3)*sind(theta));

    A = S(1,1)+S(2,2)-2*(S(1,1)-S(2,2))*cosd(2*theta)...
        -4*S(1,2)*sind(2*theta)-Pp+Sz;

    B = S(1,1)+S(2,2)-2*(S(1,1)-S(2,2))*cosd(2*theta)...
        -4*S(1,2)*sind(2*theta)-Pp-Sz;

    C = 4*Ttz^2;

    aa = ((2*sqrt(2))/3)*(C_0/((tand(Fr))^2+1));

    bb = ((2*sqrt(2))/3)*(((tand(Fr))^2-1)/((tand(Fr))^2+1));

% ----- %

fun = @(x) (1/3)*sqrt((0.5*(A-x)-0.5*sqrt((B-x)^2+C)+Pp-x)^2+...
    (0.5*(x-A)-0.5*sqrt((B-x)^2+C)-Pp+x)^2+...
    (B-x)^2+C)-aa-0.5*bb*(0.5*(A-x)+0.5*sqrt((B-x)^2+C)-Pp+x);

a = 22;
b = 34;
TolMax = 0.01;
c = Bisection(fun,a,b,TolMax);

% ----- %

M(1,i) = c;

```

```
end
Pm_min = max(M)/(0.00981*Depth);
end
```

B.3.4 Bisection method

```
%Bisection method!
% ----- %
function [c] = Bisection(fun,a,b,TolMax)
ya = fun(a);
yb = fun(b);
if ya*yb > 0
    while ya*yb > 0
        b=b+1;
        yb = fun(b);
    end
end
max1=1+round((log(b-a)-log(TolMax))/log(2));
for k = 1:max1
    c = (a+b)/2;
    yc = fun(c);
    if yc==0
        a = c;
        b = c;
    elseif yb*yc > 0
        b = c;
        yb = yc;
    else
        a=c;
        ya = yc;
    end
    if b-a < TolMax
        return
    end
end
end
c = (a+b)/2;
end
```

B.4 Main script

```

%Main script for plotting the required mud weight in order to avoid
%collapse failure initiation.
% ----- %
close all
clear variables
clc
% ----- %

%Variables and constants:
Depth = 2500;    %TVD in [m]
SH = 45;        %Maximum horizontal stress [MPa]
Sh = 45;        %Maximum horizontal stress [MPa]
Sv = 50;        %Vertical stress [MPa]
Pp = 30;

aaa = 30;       %Az of Maximum horizontal stress & geographic north [deg]
                %(alpha)
bbb = 0;        %(beta)
ggg = 0;        %(gamma)

C_0 = 13;       %Uniaxial compressive strength [MPa]
fish = 0.17;    %Poissons ratio
muint = 14.9;   %Angle of internal friction [deg]
% ----- %
%When principal stresses are unknown use the approximationn below and
%choose a value for maximum horizontal in situ stress greater than the
%minimum horizontal in situ stress.
% ----- %
%Sv = Depth * 10^(-3) * 20;
%if Depth < 3500
%  Sh = 0.0053*Depth^(1.145)+ 0.46*(Pp-1025*9.81*Depth*10^(-6));
%else
%  Sh = 0.0264*Depth-31.7+0.46*(Pp-1025*9.81*Depth*10^(-6));
%end
% ----- %

```

```

S=stress2tensor (SH, Sh, Sv);

X=zeros (1, 32400);
Y=zeros (1, 32400);
Z=zeros (1, 32400);

delta=linspace (0, 360, 180);
phi=linspace (0, 90, 180);

m=length (delta);
n=length (phi);
k=0;
h = waitbar (0, 'Compiling');
for i = 1:m
    Az=delta (i);

    for j = 1:n
        Inc=phi (j);

        X (j+k)= cosd (Az) *cosd (90-Inc);
        Y (j+k)= sind (Az) *cosd (90-Inc);
% ----- %
%Insert required.Pm function for Mohr-Coulomb calculations using newtons
%method, R_pmBis function for Mohr-Coulomb calculations using the bisection
%method (slower) or MogiCol function for Mogi-Coulomb calculations below:
% ----- %
        Z (j+k)= required.Pm (S, Pp, fish, muint, aaa, bbb, ggg, Az, Inc, C_0, Depth);
% ----- %
    end
    k=k+180;
    waitbar (i/m)
end
close (h)

% ----- %
%Plot set up below:
% ----- %

```

```
xG = linspace(-1.4,1.4,200);
yG = linspace(-1.4,1.4,200);

[xGrid,yGrid] = meshgrid(xG,yG);
LALA = griddata(X,Y,Z,xGrid,yGrid,'cubic');

contourf(xGrid,yGrid,LALA);
colormap(jet)
colorbar()
axis off
axis equal
title('Required mud weight to avoid collapse in sg. ');
hold on

rev = linspace(0, 2*pi, 50).';
R=linspace((1/3),1,3);
plot(cos(rev)*R, sin(rev)*R);

hold on

line([-1 1],[0 0]);
line([0 0],[-1 1]);
line([-cosd(30) cosd(30)],[sind(210) sind(30)]);
line([-cosd(60) cosd(60)],[sind(240) sind(60)]);
line([-cosd(30) cosd(30)],[sind(150) sind(330)]);
line([-cosd(60) cosd(60)],[sind(120) sind(300)]);

text(0,1.1,'North')
text(1.1,0,'East')

degrad = (aaa+90)*(pi/180);
[X1,Y1] = pol2cart(degrad,1.2);
[X2,Y2] = pol2cart(degrad,1);

line([X1 X2],[Y1 Y2]);
text(X1,Y1,'\sigma.H');
```

Appendix C Rock properties

Table C1: Rock properties extracted from [Fjær et al., 2008, p. 438]

Material	Density ρ 10^3 (kg/m ³)	Young's modulus E (GPa)	Poisson's ratio ν	Unconf. compr. strength C_0 (MPa)	Tensile strength T_0 (MPa)
Red Wildmoor [⊥] sandstone	1.9–2.0	1.8		14	0.4–0.7
Weak reservoir sandstone (North Sea)	1.9	0.4	0.45	1	
Berea sandstone	2.18	20	0.38	74	
St. Peter sandstone	2.34	4–10	0.05–0.10	37	
Weak shale (North Sea)	2.35	1		6	
Pierre shale I	2.37–2.39	0.77–1.12	0.35–0.37	7.5–13.9	
Shale (El Paso)	2.47	26	0.10	115	
Bedford limestone	2.21	29	0.29	51	1.6
Solenhofen limestone	2.62	64	0.29	245	4.0
Hackensack siltstone	2.59	26	0.22	123	3.0
Nevada Tuff	1.61	5.0	0.21	24	1.4
Rock salt (Diamond crystal)	2.16	5	>0.5	21	0.8
Schist [⊥] (Luther Falls)	2.81	21	0.31	55	0.6
	2.82	58	0.18	83	5.2

[⊥]Loaded perpendicular to bedding.

^{||}Loaded parallel to bedding.